Numerical Computations of Interior Transmission Eigenvalues for Scattering Objects with Cavities

Stefan Peters* Andreas Kleefeld †

February 5, 2016

Abstract

In this article we extend the inside-outside duality for acoustic transmission eigenvalue problems by allowing scattering objects that may contain cavities. In this context we provide the functional analytical framework necessary to transfer the techniques that have been used in [22] to derive the inside-outside duality. Additionally, extensive numerical results are presented to show that we are able to successfully detect interior transmission eigenvalues with the inside-outside duality approach for a variety of obstacles with and without cavities in three dimensions. In this context, we also discuss the advantages and disadvantages of the inside-outside duality approach from a numerical point of view. Furthermore we derive the integral equations necessary to extend the algorithm in [27] to compute highly accurate interior transmission eigenvalues for scattering objects with cavities, which we will then use as reference values to examine the accuracy of the inside-outside duality algorithm.

1 Introduction

The interior transmission problem arises in inverse acoustic scattering theory and has first been introduced by Kirsch [19] in 1986 and by Colton and Monk [10] in 1988. Starting with those two articles, studies such as [3, 11, 8, 15, 19, 37] focused on the discreteness of such interior transmission eigenvalues and [6, 36] were able to show the existence. Their proofs are of considerable importance, because the linear sampling method is not justified to work from the theoretical point of view for wave numbers that are interior transmission eigenvalues. We refer the reader to Cakoni & Colton [2] for an introduction to the linear sampling method. Since this historical overview is by far not complete, we refer the interested reader to the recent historical overview by Cakoni & Haddar [5] and the recent special issue by them [4]. Note that there are many open questions both from the theoretical and practical point of view (see [5, page 574]). The topic is still an active research subject in inverse scattering theory.

The numerical calculation of interior transmission eigenvalues is a challenging task, since the problem is neither elliptic nor self-adjoint. However, the knowledge of such interior transmission eigenvalues provides important information about the scatterer, for example if there are cavities inside a homogeneous material or not. This is a desired task in nondestructive testing and therefore of enormous potential interest. Actually, the interior transmission eigenvalues also provide information regarding the size and the location of the inclusion, since they satisfy a monotonicity principle (see [5]). Precisely, whenever a test anomaly is situated inside a target anomaly (to be detected), then all interior transmission eigenvalues of the obstacle containing the test anomaly are smaller than

*Center for Industrial Mathematics, University of Bremen, Bremen, Germany

†Center for Numerical Analysis and Scientific Computing, Brandenburg University of Technology, Cottbus, Germany

the interior transmission eigenvalues of the obstacle containing the target anomaly. Hence, they can be used for a method that localizes inclusions including their approximate shape by pre-computing the interior transmission eigenvalues for an obstacle with many different test anomalies and then compare those with the interior transmission eigenvalues of an obstacle with unknown cavities (see [39] for the monotonicity imaging method for magnetic induction tomography). Therefore, one needs on the one hand an efficient method that is able to calculate interior transmission eigenvalues for obstacles containing a cavity at different locations and on the other hand a method that is able to calculate those from measured far-field data. Currently, there are only a few methods that are able to compute interior transmission eigenvalues such as [12] using boundary integral equations, [22, 31] using the inside-outside duality approach, and [16, 17, 35, 38] using finite elements and variants of it. An efficient method is the one by Kleefeld [27] which is able to compute highly accurate interior transmission eigenvalues for homogeneous obstacles via a boundary element collocation method, but the scatterers surface has to be given. Herewith we are able to provide a straightforward extension to this approach. A method which does not rely on the knowledge of the obstacle is given by the inside-outside duality approach. The main focus of this paper is the extension of the inside-outside duality approach of Kirsch & Lechleiter [22] to obstacles containing cavities. Hence, we would be able to provide both ingredients for the above mentioned method.

The inside-outside duality is a technique that provides a link between interior eigenvalues and the far field data of a corresponding scattering problem. In the case of acoustic scattering by impenetrable scattering objects, this technique can be used to fully characterize interior Dirichlet, Neumann, and Robin eigenvalues of the scattering object by examining the behavior of the eigenvalues of a far field operator, arising from the corresponding scattering problem, see [14, 31]. The inside-outside duality also transfers to acoustic and electromagnetic scattering from penetrable scattering objects, where it can be used to characterize interior transmission eigenvalues that correspond to the scattering problem. In these cases however, a full characterization of interior transmission eigenvalues by this technique has so far only been proven under certain conditions to the material parameters [22, 33, 32].

In this article we want to extend the inside-outside duality to acoustic scattering from scattering objects that may contain cavities. While the techniques that have been used in [22] transfer to this problem, the main challenge consists in providing the necessary functional analytical framework to apply these techniques. In this context it is particularly important to choose the correct function spaces for the analysis, where we will mainly rely on [13]. From the numerical point of view, the inside-outside duality has been tested in [22] for acoustic scattering from a penetrable ball by analytically calculating far field data. In our numerical experiments we show that the inside-outside duality also works for a variety of other scattering objects, which may or may not contain cavities. In this context we also discuss the advantages and shortcomings of the inside-outside duality approach from a numerical viewpoint.

To indicate our main result, consider a scatterer $D \subset \mathbb{R}^3$, which is described by a function $n \in L^\infty(D)$, so that $n \geq 1$ inside of D and $n = 1$ in the exterior of D. In this setting we consider the following scattering problem: For an incident wave $u^i = e^{ikx\cdot\theta}$ with direction $\theta \in \mathbb{S}^2 := \{x \in \mathbb{R}^3 : |x| = 1\}$ we seek a total field u that solves

$$\Delta u + k^2 n u = 0 \qquad \text{in } \mathbb{R}^3, \tag{1}$$

so that the scattered field $u^s = u - u^i$ fulfills Sommerfeld's radiation condition, i.e.

$$\frac{\partial u^s(x)}{\partial r} - \mathrm{i}k u^s(x) = \mathcal{O}(r^{-2}), \qquad r = |x| \to \infty.$$

Due to the radiation condition, the scattered field u^s has the asymptotic behavior

$$u^s(x) = \frac{e^{ikr}}{4\pi r} u^\infty(\hat{x}, \theta) + O(r^{-3/2})$$

as $r \to \infty$ uniformly in $\hat{x} := x/|x| \in \mathbb{S}^2$, where u^∞ is the far field pattern of the scattered field u^s. We define the far field operator $F : L^2(\mathbb{S}^2) \to L^2(\mathbb{S}^2)$ by

$$(Fg)(\hat{x}) := \int_{\mathbb{S}^2} u^\infty(\hat{x}, \theta) g(\theta) \, \mathrm{d}\theta. \tag{2}$$

From the smoothness of its kernel, it is clear that F is compact. Furthermore normality and the well-known structure of its eigenvalues are still preserved in the case of domains with cavities [9]. More precisely, the eigenvalues $(\lambda_n)_{n\in\mathbb{N}}$ of F lie on a circle in the complex plane with radius $8\pi^2/k$ and center point $\mathrm{i}8\pi^2/k$.

Finally we introduce the transmission eigenvalue problem. A squared wavenumber k^2 is called a transmission eigenvalue if there are non-trivial functions $v, w \in L^2(D),\ v - w \in H^2(D)$, which solve the following so-called transmission eigenvalue problem

$$\begin{aligned} \Delta w + k^2 n w = 0 \quad &\text{in } D, \qquad \Delta v + k^2 v = 0 \qquad \text{in } D, \\ w = v \quad &\text{on } \Gamma_1, \qquad \frac{\partial w}{\partial \nu} = \frac{\partial v}{\partial \nu} \qquad \text{on } \Gamma_1, \end{aligned} \tag{3}$$

in an distributional sense, i.e.

$$\int_D v(\Delta\phi + k^2\phi) \ \mathrm{d}x = 0, \quad \int_D w(\Delta\phi + k^2 n\phi) \ \mathrm{d}x = 0 \quad \forall \phi \in C_0^\infty(D).$$

This transmission eigenvalue problem will be the cornerstone of all further examinations. In particular we want to prove that the behavior of the eigenvalues of F characterizes the transmission eigenvalues. Now we can indicate our main result. First we will represent the eigenvalues λ_n of the far field operator F in polar coordinates,

$$\lambda_n = |\lambda_n| e^{i\mu_n}, \qquad \mu_n \in [0, \pi),$$

so that each eigenvalue λ_n corresponds to a phase μ_n. Note that if $\lambda_n = 0$, we set $\mu_n = 0$. As we will see in Lemma 4, the eigenvalues converge to zero from the right side. This implies that there is one eigenvalue λ^* with a largest phase $\mu^* := \max_{n\in\mathbb{N}} \mu_n$. To indicate our main results from Theorem 6 and Theorem 10, note that the far field operator $F = F_k$, its eigenvalues $\lambda_n = \lambda_n(k)$ and their phases $\mu_n = \mu_n(k)$ depend on the wave number k. Then it holds that if there is a wave number k_0 so that $\mu^*(k) \to \pi$ for $k \to k_0$, then k_0^2 is a transmission eigenvalue. Furthermore if k_0^2 is a transmission eigenvalue, then, assuming that the value α in (20) does not vanish, the phase $\mu^*(k)$ converges to π for $k \to k_0$. Note that for the special case of objects containing no cavities, it has be shown for certain material parameters in [22, Section 6] that α is indeed not equal to zero. However it remains an open question how to prove this for scattering objects that contain cavities.

The remainder of this article is structured as follows: In Section 2 we will prove a factorization of the far field operator and by examining the properties of the arising operators provide a link to the transmission eigenvalue problem. In Section 3 we will establish the inside-outside duality and in particular specify the condition for which a full characterization of transmission eigenvalue can be obtained. Section 4 is then dedicated to the numerical experiments. First we will discuss the different scattering objects under consideration. Then we derive the boundary integration equations necessary to numerically generate far field data. Finally we will use this data to test the inside-outside duality for the scattering objects under consideration.

2 Linking Transmission Eigenvalues to Far Field Data

As we stated in the beginning, we want to characterize transmission eigenvalues by the behavior of the eigenvalues of the far field operator F. To this end, we first need to derive a suitable factorization

for F. As a first step we will state problem (1) more precisely. We assume that the scattering object $D \subset \mathbb{R}^3$ is simply connected with boundary $\Gamma_1 \in C^2$. Inside of D we consider a region $D_0 \subset D$, which can be multiple connected, such that $D \setminus \overline{D_0}$ is connected and assume that its boundary Γ_2 is also a C^2 curve. In the following ν denotes the outward normal to Γ_1 or Γ_2. The scattering object is described by a real-valued function n, where $n = q + 1$ for a contrast function $q \in L^\infty(D)$, such that $q \geq c_0 > 0$ in $D \setminus \overline{D_0}$ and $q = 0$ almost everywhere in D_0, where c_0 is a positive constant. Extending q by zero outside of the scattering object D, we can state the variational formulation of the scattering problem for the scattered field: We seek a function $u^s \in H^1_{\mathrm{loc}}(\mathbb{R}^3)$, such that

$$\int_{\mathbb{R}^3} \left(\nabla u^s \cdot \nabla \overline{\psi} - k^2(1+q)v\overline{\psi}\right) \, \mathrm{d}x = -\int_D k^2 q u^i \overline{\psi} \, \mathrm{d}x = -\int_{D\setminus\overline{D_0}} k^2 q u^i \overline{\psi} \, \mathrm{d}x \tag{4}$$

for all test functions $\psi \in H^1_{\mathrm{loc}}(\mathbb{R}^3)$ with compact support. The existence and uniqueness of a solution has been established in [9]. In a first step we will now prove a factorization of the far field operator. The operators in this factorization will later provide us with the necessary link to the transmission eigenvalue problem. For that purpose we introduce the Herglotz wave operator $H : L^2(\mathbb{S}^2) \to L^2(D \setminus \overline{D_0})$ by

$$(H\psi)(x) = \int_{\mathbb{S}^2} \psi(\theta) e^{ikx\cdot\theta} \, \mathrm{d}s(\theta), \quad x \in D \setminus \overline{D_0}.$$

Its adjoint $H^* : L^2(D \setminus \overline{D_0}) \to L^2(\mathbb{S}^2)$ is then given by

$$H^*(\psi)(x) = \int_{D\setminus\overline{D_0}} \psi(\theta) e^{-ikx\cdot\theta} \, \mathrm{d}s(\theta), \quad x \in \mathbb{S}^2,$$

which is the far field w^∞ of the volume potential

$$w(x) = \int_{D\setminus\overline{D_0}} \psi(y)\Phi(x,y) \, \mathrm{d}y, \qquad x \in \mathbb{R}^3.$$

Due to the properties of the fundamental solution $\Phi(x,y) = e^{ikx\cdot y}/|x-y|, x \neq y$, it holds that w is a radiating solution to $\Delta w + k^2 w = -\psi$ in $\mathbb{R}^3$. Finally we introduce the operator $T : L^2(D \setminus \overline{D_0}) \to L^2(D \setminus \overline{D_0})$ by $Tf = k^2 q(f + v|_{D\setminus\overline{D_0}})$, where $v \in H^1_{\mathrm{loc}}(\mathbb{R}^3)$ is the radiating weak solution to

$$\Delta v + k^2(1+q)v = -k^2 q f \quad \text{in } \mathbb{R}^3, \tag{5}$$

i.e.

$$\int_{\mathbb{R}^3} \nabla v \cdot \nabla \overline{\psi} - k^2(1+q)v\overline{\psi} \, \mathrm{d}x = \int_{D\setminus\overline{D_0}} k^2 q f \overline{\psi} \, \mathrm{d}x \tag{6}$$

for all $\psi \in H^1_{\mathrm{loc}}(\mathbb{R}^3)$ with compact support. Uniqueness and existence of the solution to (6) has already been established in [20]. We can now state the following factorization.

Lemma 1. *(a) The far field operator can be factorized as $F = -H^*TH$.*
(b) It holds that $T = k^2 q(\mathrm{Id} + C)$, where Id *is the identity operator and $C : L^2(D \setminus \overline{D_0}) \to L^2(D \setminus \overline{D_0})$ is a compact operator.*
(c) $\mathrm{Im}\,(Tf, f)_{L^2(D\setminus\overline{D_0})} \geq 0$ *for all $f \in L^2(D \setminus \overline{D_0})$.*

For a proof we refer to the proof of [22, Theorem 2.5], where this assertion has been proven for scattering object without cavities. The arguments transfer one-to-one to this case.

Linking transmission eigenvalues to the eigenvalues of the far field operator is possible by using the properties of the middle operator T in the latter factorization. In order to reduce our analysis to

the properties of this middle operator, we will in a first step characterize the image of the Herglotz wave operator H, which will help us to neglect this operator later on and focus on the properties of T. The image of the Herglotz operator H consists of those functions in $L^2(D \setminus \overline{D_0})$, which have an extension to D that solves the Helmholtz equation. In order to prove this, we need to introduce some technical details. First we define

$$L^2_\Delta(D) := \{w \in L^2(D),\ \Delta w \in L^2(D)\},$$

where Δw is the weak Laplacian, i.e. there exists $\eta \in L^2(D)$, so that $\int_D \eta v \ \mathrm{d}x = \int_D w \Delta v \ \mathrm{d}x$ for all $v \in C_0^\infty(D)$ and $\Delta w = \eta$. This space is equipped with the graph norm

$$\|w\|_{L^2_\Delta(D)} := \|w\|_{L^2(D)} + \|\Delta w\|_{L^2(D)}. \tag{7}$$

Let now $u \in L^2(D)$ be a distributional solution to the Helmholtz equation,

$$\int_D u(\Delta\psi + k^2\psi) \ \mathrm{d}x = 0 \qquad \forall \psi \in C_0^\infty(D). \tag{8}$$

Then it is obvious that $u \in L^2_\Delta(D)$. We follow [13, Section 3] and use Green's second identity to define the Dirichlet trace $\gamma_D u := u|_{\Gamma_1} \in H^{-1/2}(\Gamma_1)$ by

$$\langle \gamma_D u, \phi\rangle_{H^{-1/2}(\Gamma_1)\times H^{1/2}(\Gamma_1)} = \int_D (u\Delta w - w\Delta u) \ \mathrm{d}x,$$

where $w \in H^2(D)$ such that $w = 0$ and $\partial w/\partial\nu = \phi$ on Γ_1. Continuity of the trace operator $\gamma_D : L^2_\Delta(D) \to H^{-1/2}(\Gamma_1)$ is due to

$$\|\gamma_D u\|_{H^{-1/2}(\Gamma_1)} := \sup_{\|\phi\|_{H^{1/2}(\Gamma_1)}=1} \langle \gamma_D u, \phi\rangle_{H^{-1/2}(\Gamma_1)\times H^{1/2}(\Gamma_1)} \le C\|u\|_{L^2_\Delta(D)}.$$

In the same manner we can define the trace of the normal derivative $\gamma_N u := \partial u/\partial\nu\big|_{\Gamma_1} \in H^{-3/2}(\Gamma_1)$ by

$$\langle \gamma_N u, \phi\rangle_{H^{-3/2}(\Gamma_1)\times H^{3/2}(\Gamma_1)} = -\int_D (u\Delta w - w\Delta u) \ \mathrm{d}x,$$

where $w \in H^2(D)$ is such that $w = \phi$ and $\partial w/\partial\nu = 0$ on Γ_1. The operator $\gamma_N : L^2_\Delta(D) \to H^{-3/2}(\Gamma_1)$ is also continuous due to

$$\|\gamma_N u\|_{H^{-3/2}(\Gamma_1)} := \sup_{\|\phi\|_{H^{3/2}(\Gamma_1)=1}} \langle \gamma_N u, \phi\rangle_{H^{-3/2}(\Gamma_1)\times H^{3/2}(\Gamma_1)} \le C\|u\|_{L^2_\Delta(D)}.$$

It is well known that H^1-solutions of the Helmholtz equation can be represented by Green's formula. In [13, Section 3], this result was extended to L^2-solutions, showing that a solution $u \in L^2_\Delta(D)$ to (8) can be written as

$$u = \mathrm{SL}\,(\gamma_N u) - \mathrm{DL}(\gamma_D u), \tag{9}$$

where $\mathrm{SL} : H^{-3/2}(\Gamma_1) \to L^2(D)$ and $\mathrm{DL} : H^{-1/2}(\Gamma_1) \to L^2(D)$ are continuous extensions of the single layer potential and the double layer potential, given by

$$(\mathrm{SL}\,\phi)(x) := \int_{\Gamma_1} \Phi(x,y)\phi(y) \ \mathrm{d}y, \qquad \text{in } \mathbb{R}^3 \setminus \Gamma_1, \tag{10}$$

$$(\mathrm{DL}\,\psi)(x) := \int_{\Gamma_1} \frac{\partial\Phi(x,y)}{\partial\nu(y)}\psi(y) \ \mathrm{d}y, \qquad \text{in } \mathbb{R}^3 \setminus \Gamma_1. \tag{11}$$

Now we introduce two different spaces $X_{D\setminus\overline{D_0}}$ and X_D, which contain those L^2-functions that are solutions to the Helmholtz equation on the domains $D\setminus\overline{D_0}$ and D:

$$X_{D\setminus\overline{D_0}} = \Big\{ w \in L^2(D\setminus\overline{D_0}) : \int_{D\setminus\overline{D_0}} w(\Delta\psi + k^2\psi)\ \mathrm{d}\boldsymbol{x} = 0 \quad \forall \psi \in C_0^\infty(D\setminus\overline{D_0}) \Big\}$$

and

$$X_D = \Big\{ W \in L^2(D) : \int_D W(\Delta\psi + k^2\psi)\ \mathrm{d}x = 0 \quad \forall \psi \in C_0^\infty(D) \Big\}.$$

The image of the Herglotz wave operator can now be characterized by a space X, which contains those functions in $L^2(D\setminus\overline{D_0})$ that have an extension which solves the Helmholtz equation in D and can therefore be seen as a kind of interpolation space between X_D and $X_{D\setminus\overline{D_0}}$. We define

$$X = \Big\{ w \in L^2(D\setminus\overline{D_0}) :\ \exists W \in X_D,\ w = W|_{D\setminus\overline{D_0}} \Big\}. \tag{12}$$

Motivated by the definition of the space X, we define an extension operator by $E : X \to X_D$ by $E(w) = W$, where $W \in X_D$ is the unique extension of w that solves the Helmholtz equation on D. Due to Green's representation theorem for L^2-solutions of the Helmholtz equation, the extension operator has the explicit representation

$$Ew(x) = \mathrm{SL}\left(\gamma_N w\right)(x) - \mathrm{DL}(\gamma_D w)(x), \qquad x \in D. \tag{13}$$

Obviously it holds that $X \subset X_{D\setminus\overline{D_0}}$. Again due to Green's representation theorem, we can write a function $w \in X_{D\setminus\overline{D_0}}$ as

$$\begin{aligned} w(x) = {} & \mathrm{DL}(\gamma_D w)(x) - \mathrm{SL}\left(\gamma_N w\right)(x) \\ & + \mathrm{DL}(w|_{\Gamma_2})(x) - \mathrm{SL}\left(\frac{\partial w}{\partial \nu}\Big|_{\Gamma_2}\right)(x) \qquad x \in D\setminus\overline{D_0}. \end{aligned}$$

Note that if $w \in X_{D\setminus\overline{D_0}} \cap X = X$, the second part of the equation is zero, since the jump of w and its normal derivative $\partial w/\partial\nu$ over Γ_2 vanish. Therefore a map $A : X_{D\setminus\overline{D_0}} \to X$ is given by

$$Aw(x) = \mathrm{DL}(\gamma_D w)(x) - \mathrm{SL}\left(\gamma_N w\right)(x), \qquad x \in D\setminus\overline{D_0}, \tag{14}$$

where $Aw = w$ for $w \in X$. We will use this operator later to define a projection onto the space X. First we characterize the image of the Herglotz operator.

Lemma 2. *It holds that* $X = \mathrm{closure}_{L^2(D\setminus\overline{D_0})}\, \mathcal{R}(H)$.

Proof. We first define an extension $\tilde{H} : L^2(\mathbb{S}^2) \to L^2(D)$ of the Herglotz operator H by

$$\tilde{H}\psi(x) = \int_{\mathbb{S}^2} e^{ikx\cdot\theta}\psi(\theta)\ \mathrm{d}\theta \qquad x \in D,$$

so that $Hg = \tilde{H}g|_{D\setminus\overline{D_0}}$. Let now $w = H\psi$ for a arbitrary function $\psi \in L^2(\mathbb{S}^2)$. Then the extension $W = \tilde{H}\psi$ solves the Helmholtz equation in D and $w = W|_{D\setminus\overline{D_0}}$ shows that $w \in X$. Next we show that the space X is closed to conclude that $\overline{\mathcal{R}(H)} \subset X$. To this end let $(w_j)_{j\in\mathbb{N}}$ be an arbitrary sequence in X, where $w_j \to w$ in $L^2(D\setminus\overline{D_0})$. We will show that $w \in X$. Due to the attributes of the space X, there is a corresponding sequence $(W_j)_{j\in\mathbb{N}} \subset X_D$ such that $W_j|_{D\setminus\overline{D_0}} = w_j$. Since each function W_j solves the Helmholtz equation in a weak sense, we know from standard regularity results, see e.g. [34], that W_j is analytic inside of D. We choose a function $\phi \in C_0^\infty(D)$, such that

$\phi = 1$ in $\overline{D_0}$ and use Green's classical representation formula for ϕW_j and partial integration to obtain for $x \in D_0$:

$$\begin{aligned} W_j(x) &= -\int_D \left[\Delta\left(\phi(y)W_j(y)\right) + k^2\phi(y)W_j(y)\right]\Phi(x,y)\ \mathrm{d}y \\ &= -\int_{D\setminus\overline{D_0}} \left[2\nabla\phi(y)\cdot\nabla W_j(y) + W_j(y)\Delta\phi(y)\right]\ \mathrm{d}y \\ &= \int_{D\setminus\overline{D_0}} W_j(y)\left[2\,\mathrm{div}\left(\nabla\phi(y)\Phi(x,y)\right) - \Delta\phi(y)\Phi(x,y)\right]\ \mathrm{d}y. \end{aligned}$$

Since $(W_j|_{D\setminus\overline{D_0}})_{j\in\mathbb{N}}$ is a Cauchy-sequence in $L^2(D\setminus\overline{D_0})$, we conclude from the last calculation that $(W_j|_{\overline{D_0}})_{j\in\mathbb{N}}$ is a Cauchy-sequence in $L^2(\overline{D_0})$. This implies that W_j is a Cauchy-sequence in X_D and since this space is closed, there is a function $W \in X_D$ such that $W_j \to W$ and $W|_{D\setminus\overline{D_0}} = w$. Therefore $w \in X$, which shows the closedness of the space X.

To complete the proof we choose an arbitrary $w \in X$ and show, that $w \in \overline{\mathcal{R}(H)}$. Since $w \in X$, it follows that there exists $W \in L^2(D)$ with $Ew = W$ and W solves the Helmholtz equation in D. Then it follows that $W \in \overline{\mathcal{R}(\tilde{H})}$. Therefore there is a sequence $W_j \subset \mathcal{R}(\tilde{H})$, so that $\|W_j - W\|_{L^2(D)} \to 0$ as $j \to \infty$. It follows that $\|W_j|_{D\setminus\overline{D_0}} - w\|_{L^2(D)} \to 0$ and as $W_j|_{D\setminus\overline{D_0}} \in \mathcal{R}(H)$, we conclude that $w \in \overline{\mathcal{R}(H)}$, which shows the assertion. □

In the following Theorem, we characterize transmission eigenvalues by the properties of the operator T. For a proof, we again refer to [22, Theorem 3.1], where this theorem has been proven for scattering objects without cavities.

Theorem 3. *(a) Let k^2 be an interior transmission eigenvalues with transmission pair $(U, W) \in L^2(D) \times L^2(D)$ and set $w := W|_{D\setminus\overline{D_0}}$. Then $w \in X$ and it holds that $(Tw, w)_{L^2(D\setminus\overline{D_0})} = 0$.*
(b) If $w \in X$ satisfies $(Tw, w)_{L^2(D\setminus\overline{D_0})} = 0$, then there exists a function $u \in L^2(D)$ such that k^2 is transmission eigenvalue with corresponding eigenpair (u, Ew). Furthermore $u - Ew \in H_0^2(D)$.

3 The Inside-Outside Duality for Acoustic Scattering

From now on the dependency of the quantities on the variable k becomes important. Therefore we write $X = X_k$, $F = F_k$, $T = T_k$, $A = A_k$ and so on. As mentioned above the eigenvalues $(\lambda_n)_{n\in\mathbb{N}}$ of the far field operator F_k lie on a circle in the complex plane with radius $8\pi^2/k$ and center point $\mathrm{i}8\pi^2/k$ and converge to zero due to the compactness of the far field operator. We can use the properties of the operator T_k from Lemma 1 to follow the arguments from [22, Lemma 4.1] and state

Lemma 4. *Let k^2 be no transmission eigenvalue. Then λ_n converges to zero from the right, i.e.* $\mathrm{Re}\,(\lambda_n) > 0$ *for $n \in \mathbb{N}$ large enough.*

We will now consider the phases μ_n of the eigenvalues λ_n of the far field operator. To this end we represent the eigenvalues in polar coordinates,

$$\lambda_n = |\lambda_n| e^{\mathrm{i}\mu_n}, \qquad \mu_n \in [0, \pi),$$

where we set the phase $\mu_n = 0$ if $\lambda_n = 0$. The particular convergence characteristic from Lemma 4 implies that there is an eigenvalue $\lambda^*(k)$ with a largest phase $\mu^*(k) = \max_{n\in\mathbb{N}} \mu_n$. Again following [22, Theorem 4.3], we can characterize this phase in the following way.

Lemma 5. *It holds that*

$$\cot \mu^*(k) = \min_{w \in X_k} \frac{\operatorname{Re}(T_k w, w)_{L^2(D\setminus\overline{D_0})}}{\operatorname{Im}(T_k w, w)_{L^2(D\setminus\overline{D_0})}}. \tag{15}$$

The following theorem states the first part of the inside-outside duality and provides a sufficient condition for the squared wavenumber k_0^2 to be a transmission eigenvalue (see [22, Theorem 6.3(b)] in combination with Lemma 5 for a proof).

Theorem 6 (Inside-outside duality - Part 1)**.** *Choose $k_0 > 0$ such that $I := (k_0 - \varepsilon, k_0 + \varepsilon) \setminus \{k_0\}$ contains no transmission eigenvalue. If it holds that $\lim_{I \ni k \to k_0} \mu^*(k) = \pi$, then k_0^2 is an interior transmission eigenvalue.*

The other part of the inside-outside duality is more difficult to prove and currently only yields a conditional characterization of transmission eigenvalues. First we need to replace the space X_k in (15) by using a projection onto this space. To define the projection, we introduce the space W as the completion of $C_0^\infty(D \setminus \overline{D_0})$ with respect to the semi-norm $\|\psi\|_W = \|(\Delta\psi + k^2\psi)\|_{L^2(D\setminus\overline{D_0})}$. Now we define $P_k : L^2(D \setminus \overline{D_0}) \to X_k$ by

$$P_k g = A_k(g - (\Delta + k^2)\hat{w}_k) \tag{16}$$

where $\hat{w}_k \in W$ is the unique solution to the W-coercive problem

$$\int_{D\setminus\overline{D_0}} (\Delta\hat{w}_k + k^2\hat{w}_k)(\Delta\psi + k^2\psi)\ \mathrm{d}x = \int_{D\setminus\overline{D_0}} g(\Delta\psi + k^2\psi)\ \mathrm{d}x \qquad \forall \psi \in W \tag{17}$$

and $A_k : X^k_{D\setminus\overline{D_0}} \to X_k$ is the map defined in (14).

Lemma 7. *The map $P_k : L^2(D) \to X_k$ is a projection operator and the derivate $\frac{\mathrm{d}}{\mathrm{d}k} P_k$ exists and is well-defined.*

Proof. To show differentiability of P_k with respect to k, note that the operator A_k essentially consists of a sum of single layer and double layer potential. From the Taylor expansion of the fundamental solution Φ_k with respect to the variable k, the differentiability of the single layer and double layer potential follows. More precisely, the series expansion of the fundamental solution is

$$\Phi_k(x,y) = \frac{e^{ik|x-y|}}{|x-y|} = \sum_{n=0}^{\infty} \frac{(ik|x-y|)^n}{n!|x-y|} = \sum_{n=0}^{\infty} \frac{i^n k^n |x-y|^{n-1}}{n!}$$

and therefore the single layer potential from (10) can be written as

$$\mathrm{SL}_k\,\phi(x) = \int_{\Gamma_1} \sum_{n=0}^{\infty} \frac{i^n k^n |x-y|^{n-1}}{n!} \phi(y)\,\mathrm{d}s(y) = \sum_{n=0}^{\infty} \frac{i^n k^n}{n!} \int_{\Gamma_1} |x-y|^{n-1}\phi(y)\,\mathrm{d}s(y).$$

Therefore differentiating with respect to k yields

$$\begin{aligned}\frac{\mathrm{d}}{\mathrm{d}k}\,\mathrm{SL}_k\,\phi(x) &= \sum_{n=0}^{\infty} \frac{n i^n k^{n-1}}{n!} \int_{\Gamma_1} |x-y|^{n-1}\phi(y)\,\mathrm{d}s(y) = \sum_{n=1}^{\infty} \frac{i^n k^{n-1}}{(n-1)!} \int_{\Gamma_1} |x-y|^{n-1}\phi(y)\,\mathrm{d}s(y) \\ &\le \sum_{n=1}^{\infty} \frac{i^n k^{n-1}}{(n-1)!} \mathrm{diam}(D)^{n-1} \|\phi\|_{L^\infty(D)} < \infty,\end{aligned}$$

which shows the well-defindness of the derivative of the single layer potential. By the same arguments, the differentiability of the double layer potential is implied. Since the function $\hat{w}_k$ is also differentiable with respect to k, it follows that the derivative of $\mathrm{d}/\,\mathrm{d}kP_k$ exists and is well-defined.

To show that P_k is a projection, we choose an arbitrary function $g \in L^2(D \setminus \overline{D_0})$. Then

$$g - (\Delta + k^2)\hat{w} \in X^k_{D\setminus\overline{D_0}}$$

due the definition of $\hat{w}$. Consequently we have that $A_k[g - (\Delta + k^2)\hat{w}] \in X_k$. Finally if the function $g \in X_k$, it solves the Helmholtz equation in $D\setminus\overline{D_0}$, which implies that the right side of (17) vanishes. The coercivity of the sesquilinearform furthermore implies that $\hat{w}_k = 0$. Therefore $P_k g = A_k g = g$ due to the properties of the map A_k. This proves the assertion. □

Using this projection, we can rewrite the expression (15), such that

$$\cot \mu^*(k) = \min_{w\in L^2(D\setminus\overline{D_0})} \frac{\operatorname{Re}\left(T_k P_k w, P_k w\right)_{L^2(D\setminus\overline{D_0})}}{\operatorname{Im}\left(T_k P_k w, P_k w\right)_{L^2(D\setminus\overline{D_0})}}.$$

After this preliminary considerations, we can derive the second part of the inside-outside duality. For that purpose, we first calculate an auxiliary derivative in Theorem 9, which allows us to give a conditional characterization of interior transmission eigenvalues. The following Lemma is a preparation for this theorem.

Lemma 8. *Let $k_0^2 > 0$ be a transmission eigenvalue with transmission eigenpair (U_0, W_0) and set $w_0 := W_0|_{D\setminus\overline{D_0}} \in X_{k_0}$. Then the map $k \to (T_k w_0, w_0)_{L^2(D\setminus\overline{D_0})}$ is differentiable in k_0 and*

$$\frac{\mathrm{d}}{\mathrm{d}k}(T_k w_0, w_0)_{L^2(D\setminus\overline{D_0})}\Big|_{k=k_0} = \frac{2}{k_0}\int_D |\nabla v_{k_0}|^2 \ \mathrm{d}x,$$

where $v_{k_0} \in H^1_0(D)$ is the radiating solution of (6) for $k = k_0$ and $f = w_0$, i.e.

$$\int_D \left(\nabla v_{k_0}\cdot\nabla\overline{\psi} - k_0^2(1+q)v_{k_0}\overline{\psi}\right)\ \mathrm{d}x = \int_{D\setminus\overline{D_0}} k_0^2 q w_0\overline{\psi}\ \mathrm{d}x \qquad \forall \psi \in H_1(D). \tag{18}$$

Proof. Due to Rellich's Identity v_{k_0} vanishes outside of D and therefore $v_{k_0} \in H^2_0(D)$. Furthermore setting $v = v_k \in H^1_{\mathrm{loc}}(\mathbb{R}^3)$ as the radiating solution to (18) for variable wavenumber k, we find that differentiating that expression yields

$$\int_D \left(\nabla v_k'\cdot\nabla\overline{\psi} - k^2(1+q)v_k'\overline{\psi}\right)\ \mathrm{d}x = 2k\left[\int_{D\setminus\overline{D_0}} q w_0\overline{\psi}\ \mathrm{d}x + \int_D (1+q)v_k\overline{\psi}\ \mathrm{d}x\right] \qquad \forall\psi\in H_1(D). \tag{19}$$

Note also that $(T_{k_0}w_0, w_0)_{L^2(D\setminus\overline{D_0})} = 0$ by Theorem 3, i.e. $\int_{D\setminus\overline{D_0}} q\left(|w_0|^2 + v_{k_0}\overline{w_0}\right)\ \mathrm{d}x = 0$. Using this equation we get

$$\frac{\mathrm{d}}{\mathrm{d}k}(T_k w_0, w_0)_{L^2(D\setminus\overline{D_0})}\big|_{k=k_0} = \frac{\mathrm{d}}{\mathrm{d}k}\int_D qk^2(w_0+v_k)\overline{w_0}\ \mathrm{d}x\Big|_{k=k_0} = k_0^2\int_{D\setminus\overline{D_0}} q v_{k_0}'\overline{w_0}\ \mathrm{d}x.$$

Eliminating w_0 from this equation by using (18) for $\psi = v_{k_0}'$ and (19) for $\psi = v_{k_0}$, we obtain that

$$\begin{aligned}\frac{\mathrm{d}}{\mathrm{d}k}(T_k w_0, w_0)_{L^2(D\setminus\overline{D_0})}\big|_{k=k_0} &= \int_D \left(\nabla\overline{v_{k_0}}\cdot\nabla v_{k_0}' - k_0^2(1+q)\overline{v_{k_0}}v_{k_0}'\right)\ \mathrm{d}x\\ &= 2k_0\int_D \left(q w_0\overline{v_{k_0}} + (1+q)v_{k_0}\overline{v_{k_0}}\right)\ \mathrm{d}x = \frac{2}{k_0}\int_D |\nabla v_{k_0}|^2\ \mathrm{d}x,\end{aligned}$$

which concludes the proof. □

We want to use this result to calculate the derivative which involves the projection P_k onto the space X_k.

Theorem 9. *Let $k_0^2 > 0$ be a transmission eigenvalue with transmission eigenpair (U_0, W_0) and set $w_0 := W_0|_{D\setminus\overline{D_0}} \in X_{k_0}$. Then the map $k \to (T_k P_k w_0, P_k w_0)_{L^2(D\setminus\overline{D_0})}$ is differentiable in k_0 and*

$$\alpha(k_0) := \frac{\mathrm{d}}{\mathrm{d}k}(T_k P_k w_0, P_k w_0)_{L^2(D\setminus\overline{D_0})}\Big|_{k=k_0} = \frac{2}{k_0}\int_D |\nabla v_{k_0}|^2 \ \mathrm{d}x + 2k_0 \ \mathrm{Re}\int_D \overline{W_0} v_{k_0} \ \mathrm{d}x, \tag{20}$$

where v_{k_0} is again the radiating solution of (18).

Proof. By definition of P_k, we have that $P_k w_0 \in X_k$, so that $w_k := E_k P_k w_0 \in L^2(D)$ solves the Helmholtz equation, i.e.

$$\int_D w_k(\Delta\psi + k^2\psi) \ \mathrm{d}x = 0 \qquad \forall \psi \in C_0^\infty(D).$$

Note also in this context that $w_{k_0} = W_0$, i.e. the extension of w_0 to D, since $w_{k_0} = E_{k_0}P_{k_0}w_0 = E_{k_0}w_0$. The projection P_k in (16) is differentiable and it is clear that $w_k' := \mathrm{d}/\,\mathrm{d}k E_k P_k w_0$ exists and solves

$$\int_D w_k'(\Delta\overline{\psi} + k^2\overline{\psi}) \ \mathrm{d}x = -2k\int_D w_k\overline{\psi} \ \mathrm{d}x \quad \forall \psi \in C_0^\infty(D). \tag{21}$$

Also due to Green's Representation Theorem, we have that for an arbitrary $P_k w_0 \in X_k$ that

$$P_k w_0(x) = \mathrm{DL}(P_k w_0|_{\Gamma_1})(x) - \mathrm{SL}\left(\frac{\partial P_k w_0}{\partial \nu}\Big|_{\Gamma_1}\right)(x), \qquad x \in D\setminus\overline{D_0}$$

and by equation (13)

$$E_k P_k w_0(x) = \mathrm{DL}(P_k w_0|_{\Gamma_1})(x) - \mathrm{SL}\left(\frac{\partial P_k w_0}{\partial \nu}\Big|_{\Gamma_1}\right)(x), \qquad x \in D.$$

Therefore it is clear, that $\mathrm{d}/\,\mathrm{d}k w_k = \mathrm{d}/\,\mathrm{d}k E_k P_k w_0|_{D\setminus\overline{D_0}} = \mathrm{d}/\,\mathrm{d}k P_k w_0$. By applying the chain rule, we obtain that

$$\begin{aligned}\frac{d}{dk}(T_k P_k w_0, w_0) &= (T_k' P_k w_0, w_0) + (T_k P_k' w_0, P_k w_0) + (T_k P_k w_0, P_k' w_0)\\ &= (T_k' P_k w_0, w_0) + \overline{(T_k^* P_k w_0, P_k' w_0)} + (T_k P_k w_0, P_k' w_0).\end{aligned}$$

To simplify this expression, we show that $T_{k_0} w_0 = T_{k_0}^* w_0$. Indeed,

$$\begin{aligned}(T_{k_0} w_0, w_0) &= (qk_0^2 w_0, w_0) + \int_{D\setminus\overline{D_0}} qk_0^2 v_{k_0}\overline{w_0} \ \mathrm{d}x = (w_0, qk_0^2 w_0) + \int_{\mathbb{R}^3} \left(\Delta\overline{v_{k_0}} + k^2(1+q)\overline{v_{k_0}}\right) v_{k_0} \ \mathrm{d}x\\ &= (w_0, qk_0^2 w_0) + \int_{\mathbb{R}^3} \left(\Delta v_{k_0} + k^2(1+q)v_{k_0}\right)\overline{v_{k_0}} \ \mathrm{d}x = (w_0, qk_0^2 w_0) + \int_{D\setminus\overline{D_0}} qk_0^2 w_0\overline{v_{k_0}} \ \mathrm{d}x\\ &= (w_0, T_{k_0} w_0).\end{aligned}$$

This yields that

$$\frac{\mathrm{d}}{\mathrm{d}k}(T_{k_0} w_0, w_0)_{L^2(D\setminus\overline{D_0})}\Big|_{k=k_0} = 2k_0\int_D |\nabla v_{k_0}|^2 \ \mathrm{d}x + 2\mathrm{Re}\,(T_{k_0} w_0, P_{k_0}' w_0).$$

Recall that $w_k' = \frac{\mathrm{d}}{\mathrm{d}k} E_k P_k w_0 \in L^2(D)$, where w_k solves the Helmholtz equation. Furthermore from the discussion above, it is clear that $w_{k_0}'|_{D\setminus\overline{D_0}} = P_{k_0}' w_0$. Since $v_{k_0} \in H_0^2(D)$, we can use (21) to obtain

$$\begin{aligned} 2\mathrm{Re}\,(T_{k_0} w_0, P_{k_0}' w_0)_{L^2(D\setminus\overline{D_0})} &= 2\ \mathrm{Re} \int\limits_{D\setminus\overline{D_0}} q k_0^2 (v_{k_0} + w_0)\overline{w_{k_0}'}\ \mathrm{d}x = 2\ \mathrm{Re} \int\limits_D (\Delta v_{k_0} + k_0^2 v_{k_0})\overline{w_{k_0}'}\ \mathrm{d}x \\ &= 2k_0\ \mathrm{Re} \int\limits_D \overline{w_{k_0}} v_{k_0}\ \mathrm{d}x = 2k_0\ \mathrm{Re} \int\limits_D E_{k_0}\overline{w_0} v_{k_0}\ \mathrm{d}x \end{aligned}$$

All in all, we get

$$\frac{\mathrm{d}}{\mathrm{d}k}(T_k P_k w_0, P_k w_0)_{L^2(D\setminus\overline{D_0})}\Big|_{k=k_0} = \frac{2}{k_0}\int\limits_D |\nabla v_{k_0}|^2\ \mathrm{d}x + 2k_0\ \mathrm{Re} \int\limits_D E_{k_0}\overline{w_0} v_{k_0}\ \mathrm{d}x.$$

Using $E_{k_0}\overline{w_0} = \overline{W_0}$ shows the assertion. □

Using the explicit expression we obtained for $\alpha(k_0)$ in the last lemma, we can state the second part of the inside-outside duality, where we refer to [22, Lemma 5.1] for a proof.

Theorem 10 (Inside-outside duality - Part 2)**.** *Let k_0^2 be a transmission eigenvalue with transmission eigenpair (U_0, W_0) and $\alpha(k_0)$ the expression defined in* (20)*. Then it follows that $\lim_{k\nearrow k_0} \mu^*(k) = \pi$ or $\lim_{k\searrow k_0} \mu^*(k) = \pi$ if $\alpha(k_0) > 0$ or $\alpha(k_0) < 0$, respectively.*

Note that in all our numerical experiments, the phase curve approaches the value π from the left side, implying that $\alpha(k_0) > 0$ might hold for all transmission eigenvalues k_0. However, it remains an open problem to prove such a characteristic.

4 Numerical results for acoustic interior transmission eigenvalues

In this section, we present numerical results of the inside-outside duality approach for the acoustic interior transmission problem for a variety of obstacles in three dimensions without and with inclusions. First, we describe the obstacles under consideration. Second, the generation of the far-field data is described. Third, the numerical approximation of the far-field operator is illustrated. Then, this approximation is used for the inside-outside duality approach which is explained shortly. Lastly, this method is used to calculate interior transmission eigenvalues for a set of different obstacles with and without inclusion.

We present five different obstacles which can be described via spherical coordinates. The spherical coordinates (ϱ, θ, ϕ) of a point in rectangular coordinates (x, y, z) are given by

$$x = \varrho\sin(\phi)\cos(\theta)\,, \qquad y = \varrho\sin(\phi)\sin(\theta)\,, \qquad z = \varrho\cos(\phi)\,,$$

where $\varrho \in [0, \infty)$ is the radial distance, $\phi \in [0, \pi]$ is the azimuthal angle, and $\theta \in [0, 2\pi]$ is the polar angle. The first surface under consideration is a unit sphere which can be obtained by picking $\varrho = 1$. The second surface is a prolate ellipsoid of revolution with semi-principle axes of length 1, 1, and 1.2; i.e., ϱ is chosen to be 1 for the x- and y-coordinates and 1.2 for the z-coordinate. The third surface is constructed by choosing $\varrho = 1.5\sqrt{0.25\sin^2(\phi) + \cos^2(\phi)}$ and it is peanut-shaped. The acorn-shaped obstacle is obtained by the choice $\varrho = 0.6\sqrt{4.25 + 2\cos(3\phi)}$ and is the fourth surface under consideration. The last surfaces is a round short cylinder. It is given by the choice $\varrho^{10} = 1/((2\sin(\phi)/3)^{10} + \cos^{10}(\phi))$. In the sequel, the five surfaces are abbreviated by **Sph**, **Eli**, **Pea**, **Aco**, and **SCyl**, respectively. In Figure 1 we show the five obstacles under consideration. Note that they have already been used before in Kleefeld [27].

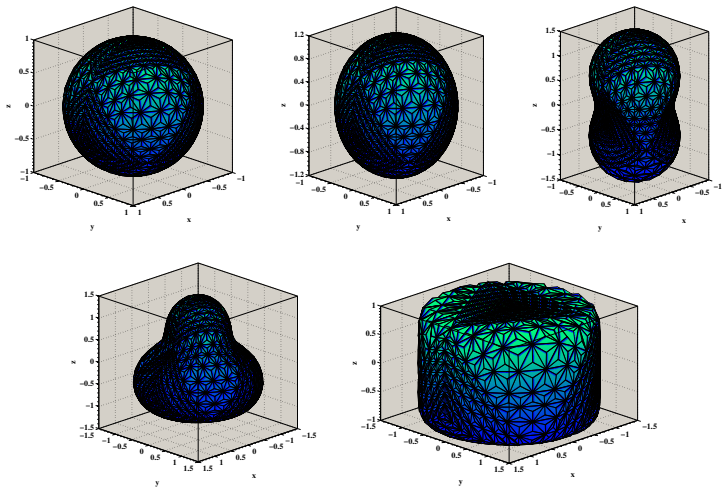

Figure 1: Left to right: **Sph**, **Eli**, **Pea**, **Aco**, and **SCyl**.

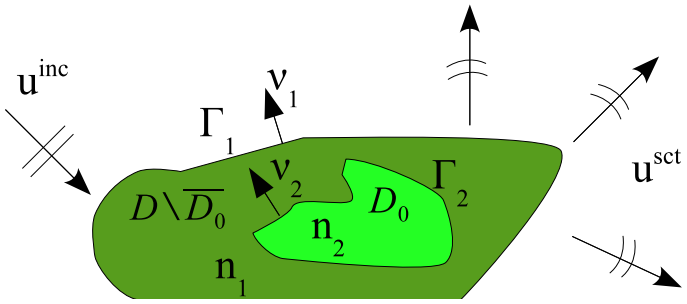

Figure 2: The setup for an acoustic scattering problem with one inclusion. An incident plane wave u^{inc} is impinging on an object $D = D \setminus \overline{D_0} \cup D_0$ with boundary Γ_1 characterized by the index of refraction n_1 containing one inclusion D_0 with boundary Γ_2 characterized by the index of refraction n_2.

4.1 Generation of far-field data for objects with an inclusion

In this subsection, it is explained how the far-field data are obtained which are needed for the numerical approximation of the far-field operator. This approximation is then used to find the interior transmission eigenvalues using the inside-outside duality approach. Here, we consider the acoustic transmission scattering problem in three dimensions for obstacles containing one inclusion.

We derive the system of boundary integral equations for solving the acoustic transmission scattering problem with one inclusion as depicted in Figure 2. We include the derivation, since the boundary value equations can also be used to extend the method in [27] to compute interior eigenvalues of known domains that contain inclusions. We use this extension in the following paragraphs to compute reference values for the ITE's that the inside-outside duality method yields. First, we need the definition of the single- and double-layer potential. They are given by

$$\mathrm{SL}_k^{\Gamma}\psi(x) = \int_{\Gamma} \Phi_k(x,y)\,\psi(y)\,\mathrm{d}s(y), \qquad x \notin \Gamma,$$

and

$$\mathrm{DL}_k^{\Gamma}\psi(x) = \int_{\Gamma} \partial_{\nu(y)}\Phi_k(x,y)\,\psi(y)\,\mathrm{d}s(y), \qquad x \notin \Gamma,$$

respectively, where Φ_k is the fundamental solution to the Helmholtz equation. We use a combination of a double- and single-layer potential in the form

$$u^{\mathrm{sct}}(x) = \mathrm{DL}_{k_{\mathrm{e}}}^{\Gamma_1}\phi_1(x) + \mathrm{SL}_{k_{\mathrm{e}}}^{\Gamma_1}\psi_1(x)\,, \qquad x \in \mathbb{R}^3\backslash\overline{D}\,, \tag{22}$$

$$u^{\mathrm{int}}(x) = \begin{cases} \mathrm{DL}_{k_1}^{\Gamma_1}\phi_1(x) + \mathrm{SL}_{k_1}^{\Gamma_1}\psi_1(x) - \mathrm{DL}_{k_1}^{\Gamma_2}\phi_2(x) - \mathrm{SL}_{k_1}^{\Gamma_2}\psi_2(x)\,, & x \in D\setminus\overline{D_0}\,, \\ \mathrm{DL}_{k_2}^{\Gamma_2}\phi_2(x) + \mathrm{SL}_{k_2}^{\Gamma_2}\psi_2(x)\,, & x \in D_0\,, \end{cases} \tag{23}$$

where $k_1 = k_{\mathrm{e}}\sqrt{n_1}$ and $k_2 = k_{\mathrm{e}}\sqrt{n_2}$ with the index of refraction $n_1 > 0$ and $n_2 > 0$ given in the domains $D\setminus\overline{D_0}$ and D_0, respectively. Here, ϕ_1, ψ_1, ϕ_2, and ψ_2 are four unknown density functions. The first two are defined on the surface Γ_1 and the last two are defined on Γ_2. Next, we define the four boundary integral operators

$$\begin{aligned} L_k^{\Gamma_i\to\Gamma_j}\psi(x) &= \int_{\Gamma_i} \Phi_k(x,y)\psi(y)\,\mathrm{d}s(y)\,, \qquad x \in \Gamma_j\,, \\ M_k^{\Gamma_i\to\Gamma_j}\psi(x) &= \int_{\Gamma_i} \partial_{\nu_i(y)}\Phi_k(x,y)\psi(y)\,\mathrm{d}s(y)\,, \qquad x \in \Gamma_j\,, \\ M_k'^{\Gamma_i\to\Gamma_j}\psi(x) &= \int_{\Gamma_i} \partial_{\nu_j(x)}\Phi_k(x,y)\psi(y)\,\mathrm{d}s(y)\,, \qquad x \in \Gamma_j\,, \\ N_k^{\Gamma_i\to\Gamma_j}\psi(x) &= \partial_{\nu_j(x)}\int_{\Gamma_i} \partial_{\nu_i(y)}\Phi_k(x,y)\psi(y)\,\mathrm{d}s(y)\,, \qquad x \in \Gamma_j\,, \end{aligned}$$

where $i,j \in \{1,2\}$. Now, we let $x \in \mathbb{R}^3\backslash\overline{D}$ approach the boundary Γ_1 in (22) and then use the jump relations to obtain

$$u^{\mathrm{sct}} = M_{k_{\mathrm{e}}}^{\Gamma_1\to\Gamma_1}\phi_1 + L_{k_{\mathrm{e}}}^{\Gamma_1\to\Gamma_1}\psi_1 + \frac{1}{2}\phi_1 \quad \text{on} \quad \Gamma_1\,.$$

Likewise, we let $x \in D\setminus\overline{D_0}$ approach the boundary Γ_1 in (23) and then use the jump relations yielding

$$u^{\mathrm{int}} = M_{k_1}^{\Gamma_1\to\Gamma_1}\phi_1 + L_{k_1}^{\Gamma_1\to\Gamma_1}\psi_1 - \frac{1}{2}\phi_1 - M_{k_1}^{\Gamma_2\to\Gamma_1}\phi_2 - L_{k_1}^{\Gamma_2\to\Gamma_1}\psi_2 \quad \text{on} \quad \Gamma_1\,.$$

Combining the last two equations via the boundary condition $u^{\mathrm{sct}} - u^{\mathrm{int}} = -u^{\mathrm{inc}}$ on Γ_1 gives

$$\phi_1 + \left(M_{k_{\mathrm{e}}}^{\Gamma_1\to\Gamma_1} - M_{k_1}^{\Gamma_1\to\Gamma_1}\right)\phi_1 + \left(L_{k_{\mathrm{e}}}^{\Gamma_1\to\Gamma_1} - L_{k_1}^{\Gamma_1\to\Gamma_1}\right)\psi_1 + M_{k_1}^{\Gamma_2\to\Gamma_1}\phi_2 + L_{k_1}^{\Gamma_2\to\Gamma_1}\psi_2 = -u^{\mathrm{inc}}\,. \tag{24}$$

Similarly, we obtain on Γ_1

$$\partial_{\nu_1}u^{\mathrm{sct}} = N_{k_{\mathrm{e}}}^{\Gamma_1\to\Gamma_1}\phi_1 + M_{k_{\mathrm{e}}}'^{\Gamma_1\to\Gamma_1}\psi_1 - \frac{1}{2}\psi_1 \quad \text{on} \quad \Gamma_1\,,$$

where we have taken the normal derivative in (22), let the point $x \in \mathbb{R}^3\backslash\overline{D}$ approach the boundary Γ_1, and used the jump relations. We also have

$$\partial_{\nu_1}u^{\mathrm{int}} = N_{k_1}^{\Gamma_1\to\Gamma_1}\phi_1 + M_{k_1}'^{\Gamma_1\to\Gamma_1}\psi_1 + \frac{1}{2}\psi_1 - N_{k_1}^{\Gamma_2\to\Gamma_1}\phi_2 - M_{k_1}'^{\Gamma_2\to\Gamma_1}\psi_2 \quad \text{on} \quad \Gamma_1\,,$$

where we have taken the normal derivative in (23), let the point $x \in D \setminus \overline{D_0}$ approach the boundary Γ_1, and used the jump relations. Using the boundary condition $\partial_{\nu_1} u^{\rm sct} - \partial_{\nu_1} u^{\rm int} = -\partial_{\nu_1} u^{\rm inc}$ on Γ_1 gives

$$-\psi_1 + \left(N_{k_{\rm e}}^{\Gamma_1\to\Gamma_1} - N_{k_1}^{\Gamma_1\to\Gamma_1}\right)\phi_1 + \left(M_{k_{\rm e}}'^{\Gamma_1\to\Gamma_1} - M_{k_1}'^{\Gamma_1\to\Gamma_1}\right)\psi_1 + N_{k_1}^{\Gamma_2\to\Gamma_1}\phi_2 + M_{k_1}'^{\Gamma_2\to\Gamma_1}\psi_2 = -\partial_{\nu_1} u^{\rm inc}\,. \quad (25)$$

The two equations (24) and (25) can be written as the system of boundary integral equations

$$\underbrace{\left(\begin{bmatrix} I & 0 \\ 0 & -I \end{bmatrix} + \begin{bmatrix} M_{k_{\rm e}}^{\Gamma_1\to\Gamma_1} - M_{k_1}^{\Gamma_1\to\Gamma_1} & L_{k_{\rm e}}^{\Gamma_1\to\Gamma_1} - L_{k_1}^{\Gamma_1\to\Gamma_1} \\ N_{k_{\rm e}}^{\Gamma_1\to\Gamma_1} - N_{k_1}^{\Gamma_1\to\Gamma_1} & M_{k_{\rm e}}'^{\Gamma_1\to\Gamma_1} - M_{k_1}'^{\Gamma_1\to\Gamma_1} \end{bmatrix}\right)}_{Z^{\Gamma_1\to\Gamma_1}} \begin{bmatrix} \phi_1 \\ \psi_1 \end{bmatrix} \quad (26)$$

$$+ \underbrace{\begin{bmatrix} M_{k_1}^{\Gamma_2\to\Gamma_1} & L_{k_1}^{\Gamma_2\to\Gamma_1} \\ N_{k_1}^{\Gamma_2\to\Gamma_1} & M_{k_1}'^{\Gamma_2\to\Gamma_1} \end{bmatrix}}_{Z^{\Gamma_2\to\Gamma_1}} \begin{bmatrix} \phi_2 \\ \psi_2 \end{bmatrix} = -\begin{bmatrix} u^{\rm inc} \\ \partial_\nu u^{\rm inc} \end{bmatrix}.$$

Next, we let $x \in D \setminus \overline{D_0}$ approach the boundary Γ_2 in (23) and then use the jump relations to obtain

$$u^{\rm int} \;=\; M_{k_1}^{\Gamma_1\to\Gamma_2}\phi_1 + L_{k_1}^{\Gamma_1\to\Gamma_2}\psi_1 - M_{k_1}^{\Gamma_2\to\Gamma_2}\phi_2 - L_{k_1}^{\Gamma_2\to\Gamma_2}\psi_2 - \frac{1}{2}\phi_2 \quad \text{on} \quad \Gamma_2\,.$$

Likewise, we let $x \in D_0$ approach the boundary Γ_2 in (23) and then use the jump relations yielding

$$u^{\rm int} \;=\; M_{k_2}^{\Gamma_2\to\Gamma_2}\phi_2 + L_{k_2}^{\Gamma_2\to\Gamma_2}\psi_2 - \frac{1}{2}\phi_2 \quad \text{on} \quad \Gamma_2\,.$$

Combining the last two equations via the boundary condition $u_+^{\rm int} - u_-^{\rm int} = 0$ on Γ_2 gives

$$M_{k_1}^{\Gamma_1\to\Gamma_2}\phi_1 + L_{k_1}^{\Gamma_1\to\Gamma_2}\psi_1 - \left(M_{k_1}^{\Gamma_2\to\Gamma_2} + M_{k_2}^{\Gamma_2\to\Gamma_2}\right)\phi_2 - \left(L_{k_1}^{\Gamma_2\to\Gamma_2} + L_{k_2}^{\Gamma_2\to\Gamma_2}\psi_2\right)\psi_2 = 0\,. \quad (27)$$

Similarly, we obtain on Γ_2

$$\partial_{\nu_2} u^{\rm int} = N_{k_1}^{\Gamma_1\to\Gamma_2}\phi_1 + M_{k_1}'^{\Gamma_1\to\Gamma_2}\psi_1 - N_{k_1}^{\Gamma_2\to\Gamma_2}\phi_2 - M_{k_1}'^{\Gamma_2\to\Gamma_2}\psi_2 + \frac{1}{2}\psi_2 \quad \text{on} \quad \Gamma_2\,,$$

where we have taken the normal derivative in (23), let the point $x \in D \setminus \overline{D_0}$ approach the boundary Γ_2, and used the jump relations. We also have

$$\partial_{\nu_2} u^{\rm int} = N_{k_2}^{\Gamma_2\to\Gamma_2}\phi_2 + M_{k_2}'^{\Gamma_2\to\Gamma_2}\psi_2 + \frac{1}{2}\psi_2 \quad \text{on} \quad \Gamma_2\,,$$

where we have taken the normal derivative in (23), let the point $x \in D_0$ approach the boundary Γ_2, and used the jump relations. Using the boundary condition $\partial_{\nu_2} u_+^{\rm int} - \partial_{\nu_2} u_-^{\rm int} = 0$ on Γ_2 gives

$$N_{k_1}^{\Gamma_1\to\Gamma_2}\phi_1 + M_{k_1}'^{\Gamma_1\to\Gamma_2}\psi_1 - \left(N_{k_1}^{\Gamma_2\to\Gamma_2} + N_{k_2}^{\Gamma_2\to\Gamma_2}\right)\phi_2 - \left(M_{k_1}'^{\Gamma_2\to\Gamma_2} + M_{k_2}'^{\Gamma_2\to\Gamma_2}\right) = 0\,. \quad (28)$$

The two equations (27) and (28) can be written as the system of boundary integral equations

$$\underbrace{\begin{bmatrix} M_{k_1}^{\Gamma_1\to\Gamma_2} & L_{k_1}^{\Gamma_1\to\Gamma_2} \\ N_{k_1}^{\Gamma_1\to\Gamma_2} & M_{k_1}'^{\Gamma_1\to\Gamma_2} \end{bmatrix}}_{Z^{\Gamma_1\to\Gamma_2}} \begin{bmatrix} \phi_1 \\ \psi_1 \end{bmatrix} \quad (29)$$

$$- \underbrace{\begin{bmatrix} M_{k_1}^{\Gamma_2\to\Gamma_2} + M_{k_2}^{\Gamma_2\to\Gamma_2} & L_{k_1}^{\Gamma_2\to\Gamma_2} + L_{k_2}^{\Gamma_2\to\Gamma_2} \\ N_{k_1}^{\Gamma_2\to\Gamma_2} + N_{k_2}^{\Gamma_2\to\Gamma_2} & M_{k_1}'^{\Gamma_2\to\Gamma_2} + M_{k_2}'^{\Gamma_2\to\Gamma_2} \end{bmatrix}}_{Z^{\Gamma_2\to\Gamma_2}} \begin{bmatrix} \phi_2 \\ \psi_2 \end{bmatrix} = \begin{bmatrix} 0 \\ 0 \end{bmatrix}.$$

Equation (29) can be isolated for the unknowns $(\phi_2, \psi_2)^{\mathrm{T}}$ as follows

$$\begin{bmatrix} \phi_2 \\ \psi_2 \end{bmatrix} = \left(Z^{\Gamma_2\to\Gamma_2}\right)^{-1} Z^{\Gamma_1\to\Gamma_2} \begin{bmatrix} \phi_1 \\ \psi_1 \end{bmatrix}.$$

Inserted into equation (26) gives

$$\left[Z^{\Gamma_1\to\Gamma_1} + Z^{\Gamma_2\to\Gamma_1}\left(Z^{\Gamma_2\to\Gamma_2}\right)^{-1} Z^{\Gamma_1\to\Gamma_2}\right] \begin{bmatrix} \phi_1 \\ \psi_1 \end{bmatrix} = - \begin{bmatrix} u^{\mathrm{inc}} \\ \partial_{\nu_1} u^{\mathrm{inc}} \end{bmatrix}. \tag{30}$$

This has to be first solved for the unknown density functions ϕ_1 and ψ_1. Then, the far-field pattern of (22) is given by

$$u^{\infty}(\hat{x};\hat{d}) = \int_{\Gamma_1} \left(\partial_{\nu_1(y)} \mathrm{e}^{-\mathrm{i}k_{\mathrm{e}}\hat{x}\cdot y}\phi_1(y) + \mathrm{e}^{-\mathrm{i}k_{\mathrm{e}}\hat{x}\cdot y}\psi_1(y)\right) \mathrm{d}s(y), \qquad \hat{x}\in\mathbb{S}^2, \tag{31}$$

where $\mathbb{S}^2$ denotes the surface of the unit sphere centered at the origin. Note that the far-field for the acoustic scattering problem without inclusion is given by (31), where ϕ_1 and ψ_1 are found by solving the 2×2 system

$$Z^{\Gamma_1\to\Gamma_1} \begin{bmatrix} \phi_1 \\ \psi_1 \end{bmatrix} = - \begin{bmatrix} u^{\mathrm{inc}} \\ \partial_{\nu_1} u^{\mathrm{inc}} \end{bmatrix},$$

which is in agreement with [1, Section 4.1]. Additionally, note that with this approach one is also able to handle more than one inclusion.

We solve numerically the system of boundary integral equations given by (30) with the superconvergent boundary element collocation solver developed in [23], which has been used in a variety of applications involving the Helmholtz equation (see for example [21, 24, 25, 26, 27, 28, 29, 30] among others). Note that all kernel of the boundary integral operator need to be weakly singular to obtain superconvergence. However, the $(2,1)$-entry of $Z^{\Gamma_2\to\Gamma_2}$ is not weakly singular. Therefore, we rewrite this entry in the form

$$\begin{aligned} & N_{k_1}^{\Gamma_2\to\Gamma_2} + N_{k_2}^{\Gamma_2\to\Gamma_2} \\ = \;& \left(N_{k_1}^{\Gamma_2\to\Gamma_2} - N_0^{\Gamma_2\to\Gamma_2}\right) + \left(N_{k_2}^{\Gamma_2\to\Gamma_2} - N_0^{\Gamma_2\to\Gamma_2}\right) + 2N_0^{\Gamma_2\to\Gamma_2} \\ = \;& \left(N_{k_1}^{\Gamma_2\to\Gamma_2} - N_0^{\Gamma_2\to\Gamma_2}\right) + \left(N_{k_2}^{\Gamma_2\to\Gamma_2} - N_0^{\Gamma_2\to\Gamma_2}\right) + 2\left(L_0^{\Gamma_2\to\Gamma_2}\right)^{-1}\left(M_0^{\Gamma_2\to\Gamma_2} M_0^{\Gamma_2\to\Gamma_2} - I/4\right) \end{aligned}$$

to get a composition of boundary integral operators each of which has a weakly singular kernel. The last step follows through the use of [9, Formula 3.12, p. 44].

Finally, we briefly mention which parameters we use to generate the far-field data for different incident waves (see [23, 30] for the description of the parameters). We use quadratic interpolation with $\alpha = 0.1$ and 1536 collocation points with the integration parameters $N_S = 128$ and $N_{NS} = 4$. In total, we use 120 different incident waves which are generated with the algorithm of Cessenat using $np = 5$ (see [7, p. 118]). Note that those waves are points which are equidistantly located on the unit sphere and denoted by

$$\hat{x}_i = \hat{d}_i, \qquad i = 1, 2, \ldots, 120. \tag{32}$$

4.2 Far field for a unit sphere containing one inclusion

In order to test the inside-outside duality, we will analytically calculate far field data for acoustic scattering by a unit ball that contains an inclusion. We can then use this data to find transmission

eigenvalues for this scattering problem and examine if those transmission eigenvalues are indeed characterized by the inside-outside duality technique. For scattering objects that are no unit ball, we will rely on the numerical computations of transmission eigenvalues that was done in [27].

To obtain analytical data, we derive a series expansion for a sphere of radius R_1 centered at the origin that contains as an inclusion a sphere of radius R_2 centered at the origin, such that it holds $0 < R_2 < R_1$. In the sequel, j_p denotes the spherical Bessel function of the first kind of order p, $h_p^{(1)}$ and $h_p^{(2)}$ the spherical Hankel function of the first and second kind of order p, P_p is the Legendre polynomial of order p, and Y_p^m is the spherical harmonic. We set $x = r\hat{x}$ with $r > 0$ and $\hat{x} \in \mathbb{S}^2$. Then we have

$$u^{\mathrm{sct}}(r\hat{x}) = \sum_{p=0}^{\infty} \sum_{m=-p}^{p} a_p^m h_p^{(1)}(k_{\mathrm{e}} r) Y_p^m(\hat{x}) \,, \quad r > R_1$$

in the exterior (see [9, Theorem 2.15]) and

$$u^{\mathrm{int}}(r\hat{x}) = \begin{cases} \sum_{p=0}^{\infty} \sum_{m=-p}^{p} \left(b_p^m h_p^{(1)}(k_{\mathrm{e}}\sqrt{n_1} r) + c_p^m h_p^{(2)}(k_{\mathrm{e}}\sqrt{n_1} r) \right) Y_p^m(\hat{x}) \,, & R_2 < r \leq R_1 \,, \\ \sum_{p=0}^{\infty} \sum_{m=-p}^{p} d_p^m j_p(k_{\mathrm{e}}\sqrt{n_2} r) Y_p^m(\hat{x}) \,, & 0 < r \leq R_2 \,, \end{cases}$$

in the interior. Using the Jacobi-Anger expansion of the incident field gives

$$u^{\mathrm{inc}}(r\hat{x}; \hat{d}) = \sum_{p=0}^{\infty} \sum_{m=-p}^{p} 4\pi \mathrm{i}^p j_p(k_{\mathrm{e}} r) Y_p^m(\hat{x}) \overline{Y_p^m(\hat{d})} \,.$$

Using the boundary conditions on the sphere $r = R_1$ and $r = R_2$, respectively, yields the algebraic system $Ax = b$ with

$$A = \begin{bmatrix} h_p^{(1)}(k_{\mathrm{e}} R_1) & -h_p^{(1)}(k_{\mathrm{e}}\sqrt{n_1} R_1) & -h_p^{(2)}(k_{\mathrm{e}}\sqrt{n_1} R_1) & 0 \\ h_p^{(1)'}(k_{\mathrm{e}} R_1) & -\sqrt{n_1} h_p^{(1)'}(k_{\mathrm{e}}\sqrt{n_1} R_1) & -h_p^{(2)'}(k_{\mathrm{e}}\sqrt{n_1} R_1) & 0 \\ 0 & h_p^{(1)}(k_{\mathrm{e}}\sqrt{n_1} R_2) & h_p^{(2)}(k_{\mathrm{e}}\sqrt{n_1} R_2) & -j_p(k_{\mathrm{e}}\sqrt{n_2} R_2) \\ 0 & \sqrt{n_1} h_p^{(1)'}(k_{\mathrm{e}}\sqrt{n_1} R_2) & \sqrt{n_1} h_p^{(2)'}(k_{\mathrm{e}}\sqrt{n_1} R_2) & -\sqrt{n_2} j_p'(k_{\mathrm{e}}\sqrt{n_2} R_2) \end{bmatrix},$$

$$x = \begin{bmatrix} a_p^m \\ b_p^m \\ c_p^m \\ d_p^m \end{bmatrix}, \qquad \text{and} \qquad b = \begin{bmatrix} -4\pi \mathrm{i}^p j_p(k_{\mathrm{e}} R_1) \overline{Y_p^m(\hat{d})} \\ -4\pi \mathrm{i}^p j_p'(k_{\mathrm{e}} R_1) \overline{Y_p^m(\hat{d})} \\ 0 \\ 0 \end{bmatrix}.$$

Next, we have to solve this system for a_p^m. Using Cramer's rule, the solution is given by the following expression

$$a_p^m = -4\pi \mathrm{i}^p \overline{Y_p^m(\hat{d})} \frac{N_p}{D_p} \,,$$

with $D_p = \det(A)$ and

$$N_p = \det \begin{bmatrix} j_p(k_{\mathrm{e}} R_1) & -h_p^{(1)}(k_{\mathrm{e}}\sqrt{n_1} R_1) & -h_p^{(2)}(k_{\mathrm{e}}\sqrt{n_1} R_1) & 0 \\ j_p'(k_{\mathrm{e}} R_1) & -\sqrt{n_1} h_p^{(1)'}(k_{\mathrm{e}}\sqrt{n_1} R_1) & -h_p^{(2)'}(k_{\mathrm{e}}\sqrt{n_1} R_1) & 0 \\ 0 & h_p^{(1)}(k_{\mathrm{e}}\sqrt{n_1} R_2) & h_p^{(2)}(k_{\mathrm{e}}\sqrt{n_1} R_2) & -j_p(k_{\mathrm{e}}\sqrt{n_2} R_2) \\ 0 & \sqrt{n_1} h_p^{(1)'}(k_{\mathrm{e}}\sqrt{n_1} R_2) & \sqrt{n_1} h_p^{(2)'}(k_{\mathrm{e}}\sqrt{n_1} R_2) & -\sqrt{n_2} j_p'(k_{\mathrm{e}}\sqrt{n_2} R_2) \end{bmatrix}, \quad (33)$$

but further simplification is avoided due to the very long expressions. Note that both determinants are only depending on p (not on m and $\hat{d}$). The far-field pattern of u^{sct} is given by the expression (see [9, Theorem 2.16] without the factor 4π which is due to a different definition of the far-field)

$$u^\infty(\hat{x};\hat{d}) \;=\; \frac{4\pi}{k_{\text{e}}}\sum_{p=0}^{\infty}\frac{1}{\mathrm{i}^{p+1}}\sum_{m=-p}^{m} a_p^m Y_p^m(\hat{x}) = \frac{4\pi\mathrm{i}}{k_{\text{e}}}\sum_{p=0}^{\infty}(2p+1)\frac{N_p}{D_p}P_p(\hat{x}\cdot\hat{d})\,.$$

The last step follows by the addition theorem for spherical harmonics (see [9, Theorem 2.9]). Finally, note that the far-field of a sphere of radius R_1 without inclusion is given by (see [27, Section 4.2] for the derivation)

$$\begin{aligned} & u^\infty(\hat{x};\hat{d}) \qquad\qquad (34)\\ = \;& \frac{4\pi\mathrm{i}}{k_{\text{e}}}\sum_{p=0}^{\infty}(2p+1)\frac{\sqrt{n_1}j_p'(k_e\sqrt{n_1}R_1)j_p(k_{\text{e}}R_1) - j_p'(k_{\text{e}}R_1)j_p(k_{\text{e}}\sqrt{n_1}R_1)}{\sqrt{n_1}j_p'(k_{\text{e}}\sqrt{n_1}R_1)h_p^{(1)}(k_{\text{e}}R_1) - h_p^{(1)'}(k_{\text{e}}R_1)j_p(k_{\text{e}}\sqrt{n_1}R_1)}P_p(\hat{x}\cdot\hat{d})\,, \end{aligned}$$

where we adopted the formula to our notations and used the additional factor 4π which is due to the different definition of the far-field pattern.

4.3 The inside-outside duality method

For the inside-outside duality we need to approximate the far field operator in (2) numerically. To this end we subdivide the unit sphere into N patches of equal size. The size of a patch is given by the surface area of the sphere 4π divided by the number of patches; i.e. $\omega = 4\pi/N$. In our experiments, we choose $N = 120$, such that $\omega = 4\pi/120 = \pi/30 \approx 0.104\,719\,755$. The midpoints of each patch are given by the points defined in (32). The numerical approximation of the integral appearing in (2) is achieved by constant interpolation over each patch. That is, we get for $i = 1, 2, \ldots, 120$

$$\begin{aligned} Fg\,(\hat{x}_i) = F_k g\,(\hat{x}_i) \;&\approx\; \sum_{j=1}^{120}\omega u^\infty(\hat{x}_i;\hat{d}_j)g(\hat{d}_j)\\ &=\; \underbrace{\omega\begin{bmatrix} u^\infty(\hat{x}_1;\hat{d}_1) & u^\infty(\hat{x}_1;\hat{d}_2) & \ldots & u^\infty(\hat{x}_1;\hat{d}_{120})\\ u^\infty(\hat{x}_2;\hat{d}_1) & u^\infty(\hat{x}_2;\hat{d}_2) & \ldots & u^\infty(\hat{x}_2;\hat{d}_{120})\\ \vdots & \vdots & & \vdots\\ u^\infty(\hat{x}_{120};\hat{d}_1) & u^\infty(\hat{x}_{120};\hat{d}_2) & \ldots & u^\infty(\hat{x}_{120};\hat{d}_{120}) \end{bmatrix}}_{F_N}\begin{bmatrix} g(\hat{d}_1)\\ g(\hat{d}_2)\\ \vdots\\ g(\hat{d}_{120}) \end{bmatrix}. \end{aligned}$$

Here, F_N is a matrix that contains all the information that is needed for the inside-outside duality approach.

To verify the inside-outside duality for acoustic scattering from Theorem 6 and 10, we compute the eigenvalues $\lambda_{j,N}, j = 1, .., 120$ of F_N as an approximation to the eigenvalues λ_j of F for a sequence of wavenumbers, suitable for the scattering object under consideration. We then examine how the corresponding phases $\mu_{j,N}$ behave with varying wave number, in particular where the phase $\mu_N^* = \max_{j=1,.,120}\mu_{j,N}$ converges to π. Note that small errors in eigenvalues close to zero lead to large errors in the corresponding phases. We therefore suggest a regularization scheme that has already shown to work well in [31, 32]. If required, we first neglect eigenvalues that are to close to zero, i.e. eigenvalues which lie in the ball $\{z \in \mathbb{C}, |z| < \varepsilon\}$, where ε is the noise level of F_N, given by $\|F_N - F\|$. In a second step we use the knowledge that the eigenvalues λ_j of F lie on a circle $\{z \in \mathbb{C}, |z - 8\pi^2\mathrm{i}/k|\}$ in the complex plane to project the numerically approximated eigenvalues $\lambda_{j,N}$ orthogonally onto this circle, using the projection mapping

$$\mathcal{P} :\, \lambda \mapsto \frac{8\pi^2\mathrm{i}}{k} + \frac{8\pi^2}{k}\frac{\lambda - 8\pi^2\mathrm{i}/k}{|\lambda - 8\pi^2\mathrm{i}/k|}. \qquad (35)$$

Although this projection might theoretically increase the phase error for certain eigenvalues $\lambda_{j,N}$, it has a stabilizing effect upon our computations and leads to data that is easier to interpret. Geometric considerations as in [18] also show that the projection operator leads to better error bounds for the phase error, in particular for eigenvalues close to zero.

We plot the phases $\mu_{j,N}^P$ of the projected eigenvalues $\mathcal{P}[\lambda_{j,N}](k)$ for a sequence of wavenumbers k_n. Note that our objective is to test the inside-outside duality under "optimal circumstances" to evaluate its advantages and shortcomings as a method. That is also why we neglected to add artifical noise and calculated far field data as precisely as possible. Effects of the influence of noise and possible regularization techniques with regard to noise are discussed in [18, 31].

A typical example for a phase plot is shown in Figure 3, where we used the inside-outside duality approach to detect transmission eigenvalues of a unit ball with constant index of refraction $n = 4$ with or without inclusion. As approximations for the transmission eigenvalues, we choose the wavenumbers that corresponds to the phases closest to π in the eigenvalue curve under consideration. This approach works particularly well if the eigenvalue curve shows a steep ascend close to π, which is the case in the example of scattering by a unit sphere, as we will discuss in the next subsection in more detail.

4.3.1 The unit sphere

In this subsection we present the numerical calculation for interior transmission eigenvalues for a unit sphere that may or may not contain an inclusion by using the inside-outside duality approach. With the results from section 4.2, we analytically calculate transmission eigenvalues for the unit sphere and then discuss the quality of the inside-outside duality approach to approximate these transmission eigenvalues. The interior transmission eigenvalues for a unit sphere without inclusion are given by the roots of the function

$$f(k) = \det \begin{bmatrix} j_p(k) & -j_p(k\sqrt{n}) \\ j_p'(k) & -\sqrt{n} j_p'(k\sqrt{n}) \end{bmatrix} \tag{36}$$

for $p \geq 0$, which is the numerator of the expression (34) (see also [27, Section 6.1] for a derivation). For the index of refraction $n = 4$, we get the first four interior transmission values 3.141 59, 3.692 45, 4.261 68, and 4.831 86 (see also [27, Table 12]), which can also be seen in the first column of Table 1, which contains analytical values for all the cases we are going to discuss in this subsection. The values are also confirmed by the use of the inside-outside duality approach, where we used the interval $[1, 5]$ and the gridsize 0.01. As one can see in Figure 3(a), we are able to detect the first four interior transmission eigenvalues. Precisely, we obtain the results 3.14, 3.69, 4.26, and 4.83 that are accurate within the chosen grid size. Note that for the first transmission eigenvalue, there are two phase curves that approach this value. Zooming into the curves shows that in the one of the two curves are two eigenvalues contained that approaches the value 3.14. The first transmission eigenvalue has multiplicity three (see also [27, Table 12]). Hence, we have to conclude that the inside-outside duality approach also takes multiplicity of transmission eigenvalues into account. Note also that the slope of the first curve approaching the first transmission eigenvalue decreases rapidly in the end. In this particular example this in no problem due to the high accuracy in computation, but we will see later that the potential flatness of eigenvalue curves leads to a decrease in accuracy for the approximation of transmission eigenvalues for other scattering objects. This is also why we avoid using the extrapolation algorithm provided in [32].

Next we use the same unit sphere with index of refraction $n_1 = 4$ but now include a cavity in form of a sphere of radius $R_1 = 0.1$ and index of refraction $n_1 = 1$. The results can be seen in Figure 3(b), from which we obtain the values 3.14, 3.49, and 3.69. Comparing this to the analytical values in the second column of Table 1 shows that we stay within the accuracy of the chosen grid size. This may

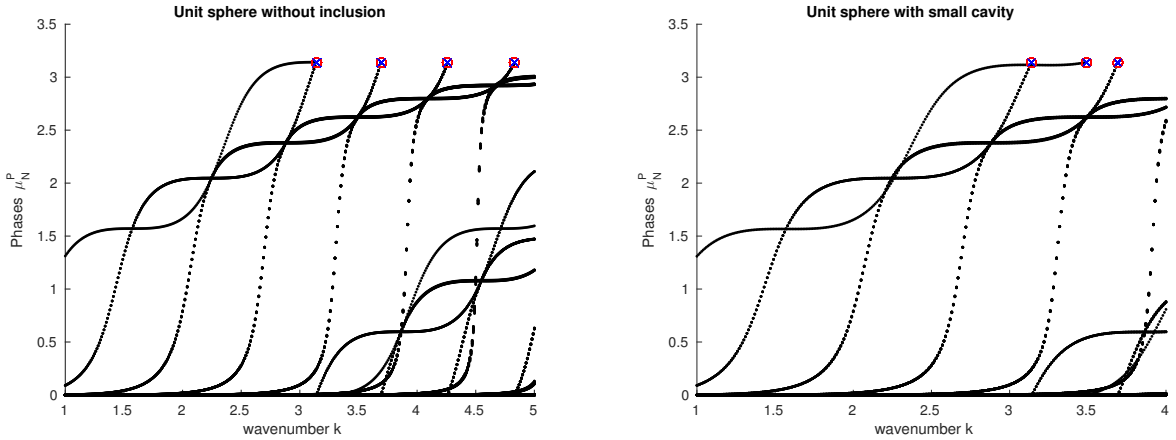

(a) 401 points for the interval 1 to 5

(b) 301 points for the interval 1 to 4

Figure 3: (a) The detection of four interior transmission eigenvalues with the inside-duality approach for a unit sphere without inclusion. (b)The detection of three interior transmission eigenvalues for a unit sphere containing a spherical cavity of radius $R = 0.1$. Blue crosses on the π axis mark the exact position of the transmission eigenvalues.

seem remarkable for the second interior transmission eigenvalue because the corresponding phase curve seems rather flat but zooming into the graph shows a definite increase in slope towards the end of the curve, allowing for a precise estimation of the transmission eigenvalue.

As a conclusion to this subsection we want to show we can also use spherical inclusions that have index of refraction different from one. We use one spherical inclusion of radius $R_2 = 0.1$ with index of refraction $n_2 = 3$ and one inclusion of radius $R_3 = 0.5$ and index of refraction $n_3 = 3$. The results can be seen in Figure 4. The graph in Figure 4(a) is similar to the case with the cavity in Figure 3(b). In particular the flatness of the second phase curve decreases towards the end of the curve, allowing for the precise estimation 3.37 of the second transmission eigenvalue within the gird size. The other two values 3.14 and 3.69 are also accurate within the chosen grid size. Hence, we are able to show that the inside-outside duality approach also works for an inclusion that has a different contrast that is not one. The same is true for the results shown in Figure 4(b). We obtain the values 3.44, 3.88. Later we will encounter obstacles for which the phase curve stays flat and an estimation of the transmission eigenvalues is more imprecise.

The parameters and the interior transmission eigenvalues are listed in Table 1 along with the results for a sphere without inclusion. The interior transmission eigenvalues are obtained by calculating numerically the zeros of the function given by (33).

ITE	no inclusion	$R_1 = 0.1$, $n_1 = 1$	$R_2 = 0.1$, $n_2 = 3$	$R_3 = 0.5$, $n_3 = 3$
1.	3.141 59	3.142 59	3.141 93	3.443 64
2.	3.692 45	3.490 66	3.373 33	3.883 18
3.	4.261 68	3.692 48	3.692 46	3.947 66
4.	4.831 86	4.261 68	4.261 68	4.382 33

Table 1: Different parameters for the unit sphere containing a sphere of different size and different index of refraction

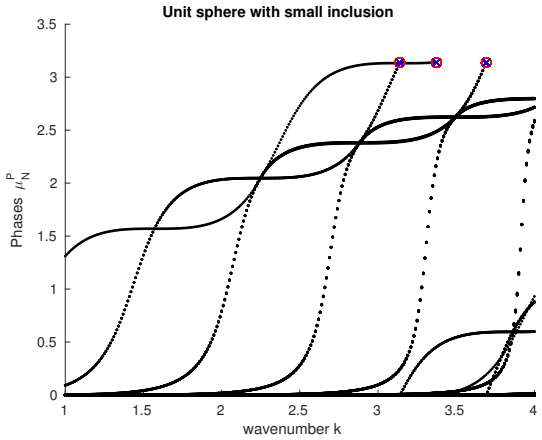

(a) 301 points for the interval 1 to 4

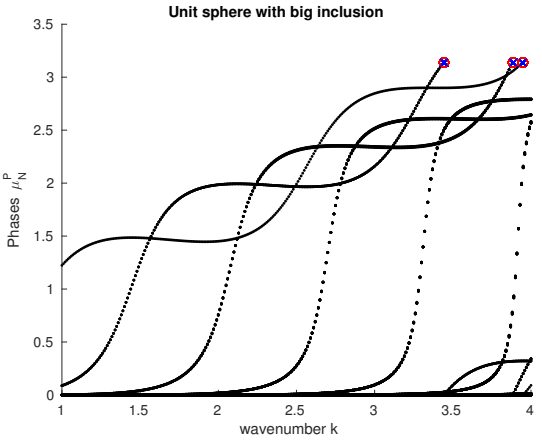

(b) 301 points for the interval 1 to 4

Figure 4: (a) The detection of three interior transmission eigenvalues with the inside-duality approach for a unit sphere with a spherical inclusion of radius $R = 0.1$ and refractive index $n = 3$. (b)The detection of three interior transmission eigenvalues for a unit sphere containing a spherical inclusion of radius $R = 0.5$ and refractive index $n = 3$. Blue crosses on the π axis mark the exact position of the transmission eigenvalues.

4.3.2 The ellipsoid

After taking a closer look at the detection of transmission eigenvalues for a sphere without inclusion and with inclusions that may or may not be cavities, we will from now on focus only on inclusions that are cavities, i.e. have refractive index of $n = 1$. We start by considering the ellipsoid as scattering object and consider the cases of an ellipsoid without cavities or with spherical cavities of size $R = 0.1$, $R = 0.2$ and $R = 0.3$. As one can see in Figure 5, the ellipsoid allows for a precise characterization of transmission eigenvalues due to the steep ascend of the eigenvalue curves. The approximations we obtain can be seen in Table 2 under the name "IO-value". As in the case of the sphere, the approximation of the transmission eigenvalues is precise within the step size of the wave number grid, except for the last value in the second column, which shows a slight deviation. Note that the six-digit reference value in Table 2 are numerically computed by the integral equation method for transmission eigenvalues, introduced in [27].

ITE ellipsoid	no inclusion	IO-value	small cavity	IO-value	bigger cavity	IO-value	biggest cavity	IO-value
1.	2.855721	2.85	2.855265	2.85	2.869239	2.86	2.937557	2.93
2.	2.931834	2.93	3.053040	3.05	3.073341	3.07	3.169967	3.16
3.	3.052080	3.05	3.095740	3.10	3.301488	3.30	3.379890	3.37

Table 2: Approximations for the first three transmission eigenvalues for the ellipsoid with the inside-outside duality.

4.3.3 The acorn

As an example for which the inside-outside duality fails in precisely detecting interior transmission eigenvalues is the scattering object acorn. As you can see in Figure 6(a) all phase curves, except for the last one, become very flat as they approach the critical value π. Zooming into the phase curve shows that in particular the third transmission eigenvalue is only approximated very roughly since the corresponding phase curve vanishes too early. The values for the first, second and fourth transmission eigenvalue are closer, but still not as precise as one would hope from the examples given

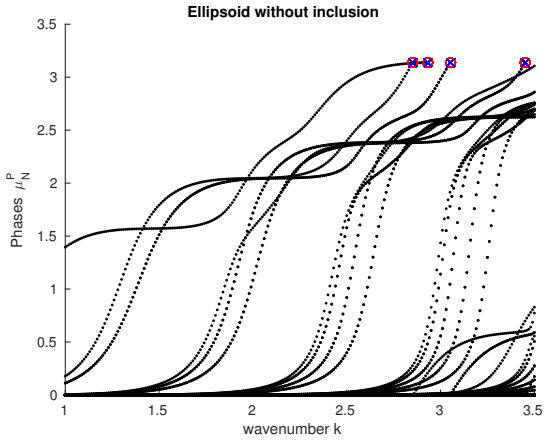

(a) 251 points for the interval 1 to 3.5

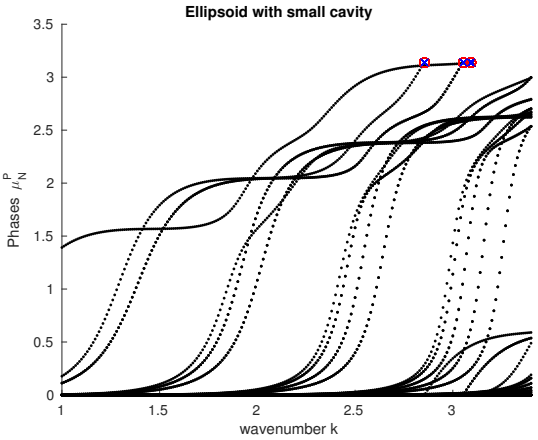

(b) 241 points for the interval 1 to 3.4

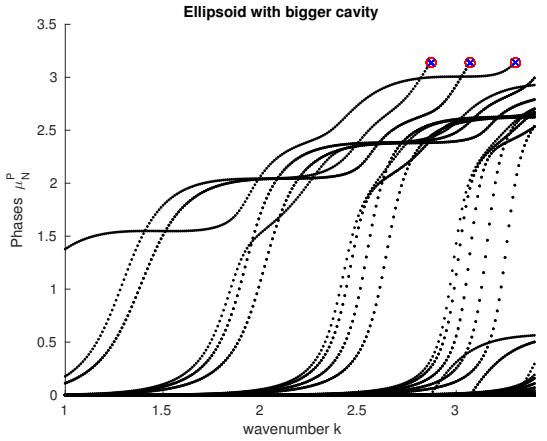

(c) 241 points for the interval 1 to 3.4

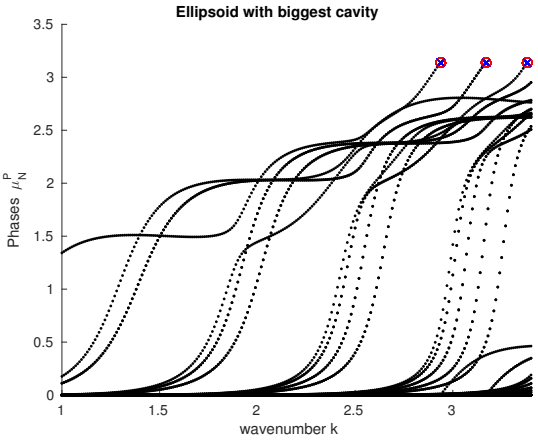

(d) 241 points for the interval 1 to 3.4

Figure 5: Detection of interior transmission eigenvalues of the ellipsoid (a) without cavity (b) with spherical cavity of radius $R = 0.1$ (c) with spherical cavity of radius $R = 0.2$ (d) with spherical cavity of radius $R = 0.3$. Blue crosses on the π axis mark the exact position of the transmission eigenvalues.

above. The problem is worsened by including a cavity into the acorn, depicted in Figure 6(b). As one can see in Table 3, only the fourth transmission eigenvalue is approximated decently. It appears that by increasing the "geometric complexity" of a scattering object, the eigenvalue curves tend to become flatter, making the inside-outside duality procedure a less than optimal tool to accurately detect interior transmission eigenvalues.

ITE short cylinder	no inclusion	IO-value	one inclusion	IO-value
1.	2.694649	2.67	2.718420	2.64
2.	2.711716	2.69	2.733531	2.67
2.	2.910972	2.83	2.941369	2.84
2.	2.986754	2.98	2.994080	2.98

Table 3: Approximations for the first four interior transmission eigenvalues for the acorn with the inside-outside duality.

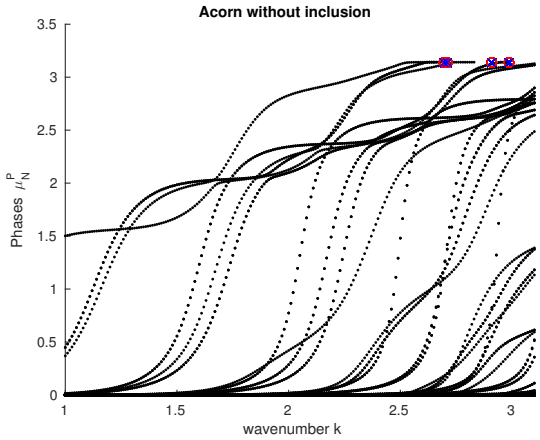

(a) 211 points for the interval 1 to 3.1

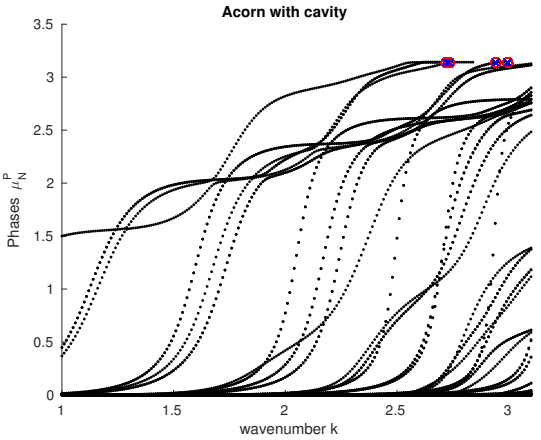

(b) 211 points for the interval 1 to 3.1

Figure 6: Detection of interior transmission eigenvalues of the acorn (a) without cavity (b) with spherical cavity of radius $R = 0.1$. Blue crosses on the π axis mark the exact position of the transmission eigenvalues.

4.3.4 The peanut

Next we consider the scattering object peanut. Here a similar difficulty arises as in the previous case where we considered the acorn. Both eigenvalue curves become rather flat but unlike in the previous case, the curves still allow an approximation of the transmission eigenvalues that is at least precise for one place after the decimal point.

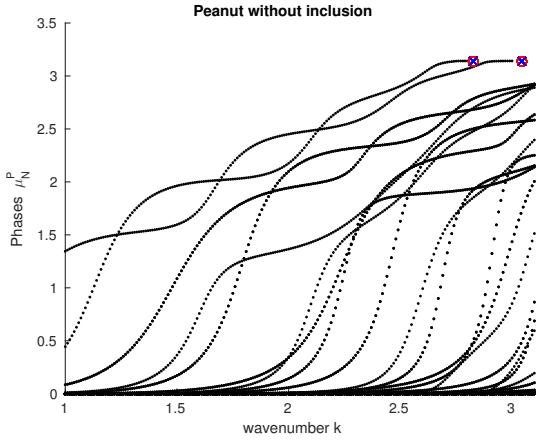

(a) 211 points for the interval 1 to 3.1

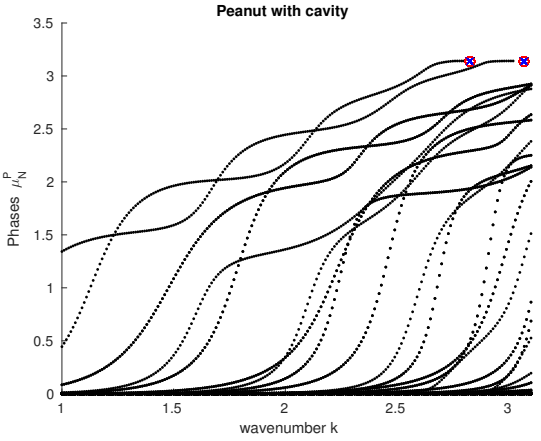

(b) 211 points for the interval 1 to 3.1

Figure 7: Detection of interior transmission eigenvalues of the peanut (a) without cavity (b) with spherical cavity of radius $R = 0.1$. Blue crosses on the π axis mark the exact position of the transmission eigenvalues.

ITE peanut	no inclusion	IO-value	one inclusion	IO-value
1.	2.825465	2.80	2.825837	2.80
2.	3.044714	3.00	3.066903	3.02

Table 4: Approximations for the first two transmission eigenvalues for the peanut with the inside-outside duality.

4.3.5 The short cylinder

As a final scattering object we will consider the short cylinder. Here the approximations of the transmission eigenvalues are again precise within the accuracy of the chosen grid size or show only very small derivations as one can see in Table 5. As we noted above, this may again be due to the decrease in "geometric complexity" of the scattering object when compared to the peanut or the acorn. In this context it would be interesting to examine if geometric complexity is an actual quantity that can be measured in a way such that it corresponds to certain behavioral patterns of the eigenvalue curves. For example one could take the surface-to-volume ratio of a scattering object as a measure for geometric complexity and conclude that since this ratio is smallest for the ball, the eigenvalue curve should have a steep ascend close to π. However it is far from obvious if such a link exists and how it could be established.

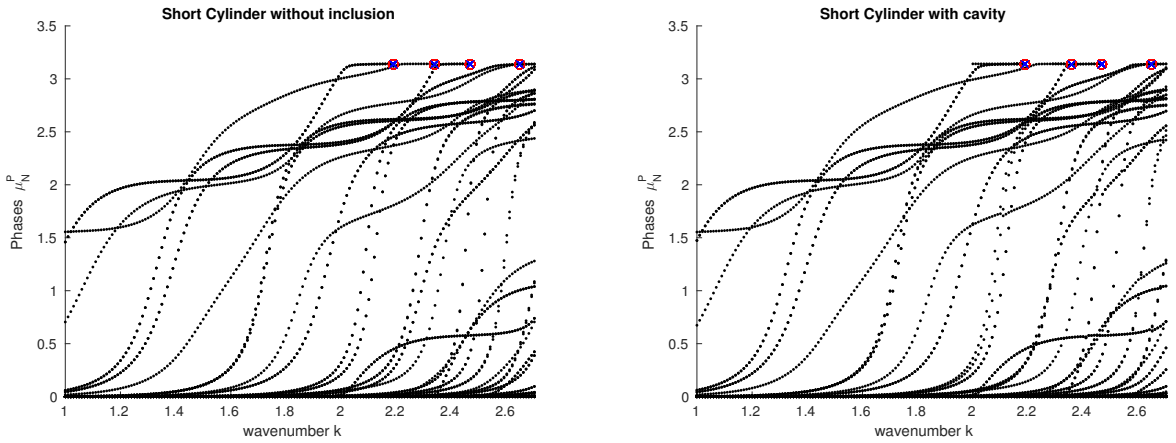

(a) 171 points for the interval 1 to 2.7

(b) 171 points for the interval 1 to 2.7

Figure 8: Detection of interior transmission eigenvalues of the short cylinder (a) without cavity (b) with spherical cavity of radius $R = 0.1$. Blue crosses on the π axis mark the exact position of the transmission eigenvalues.

ITE short cylinder	no inclusion	IO-value	one inclusion	IO-value
1.	2.187215	2.18	2.187329	2.18
2.	2.337717	2.33	2.357965	2.34
3.	2.468408	2.46	2.468410	2.46
4.	2.645202	2.64	2.645487	2.65

Table 5: Approximations for the first four transmission eigenvalues for the short cylinder with the inside-outside duality.

5 Conclusion and Outlook

The theoretical and practical approach we have chosen to determine interior transmission eigenvalues from far field data works reasonably well. We were able to theoretically characterize interior transmission eigenvalues and to turn the theoretical results into a working algorithm that is able to detect interior transmission eigenvalues for a variety of scattering objects in three dimensions. However, there are still some open questions to be answered from both the theoretical and the numerical point of view. From the theoretical point of view, it would be desirable to obtain an explicit value for the derivative α in (20) to make sure this value is different from zero, independent of the material parameters involved. This would then lead to a full characterization of interior transmission eigenvalues by the inside-outside duality. Furthermore, it would be interesting to derive the inside-outside duality also for scattering objects with cavities for either electromagnetic or elastic scattering.

From the numerical point of view, the main question is how to deal with the flatness of certain phase curve in the proximity of the critical value π. In particular, it would be helpful to find a criterion which shows a relation between the slope of phase curves close the π and the geometry of the scattering object in order to be able to give a regularization scheme, dependent on the flatness of certain phase curves. We hope to be able to provide an answer to both the theoretical and numerical questions to some extent in future work.

6 Acknowledgments

The research of SP was supported through an exploratory project granted by the University of Bremen in the framework of its institutional strategy, funded by the excellence initiative of the federal and state governments of Germany.

References

[1] K. A. Anagnostopoulos, A. Charalambopoulos, and A. Kleefeld. The factorization method for the acoustic transmission problem. *Inverse Problems*, 29(11):115015, 2013.

[2] F. Cakoni and D. Colton. *Qualitative Methods in Inverse Scattering Theory. An Introduction.* Springer, Berlin, 2006.

[3] F. Cakoni and H. Haddar. On the existence of transmission eigenvalues in an inhomogeneous medium. *Appl. Anal.*, 88(4):475–493, 2009.

[4] F. Cakoni and H. Haddar. Transmission eigenvalues [Editorial]. *Inverse Problems*, 29(10):100201, 3, 2013.

[5] F. Cakoni and H. Haddar. Transmission eigenvalues in inverse scattering theory. 60:529–580, 2013.

[6] F. Cakoni, H. Haddar, and D. Gintides. The existence of an infinite discrete set of transmission eigenvalues. *SIAM J. Math. Anal.*, 42:237–255, 2010.

[7] O. Cessenat. *Application d'une nouvelle formulation variationnelle aux équations d'ondes harmoniques. Problèmes de Helmholtz 2D et de Maxwell 3D.* PhD thesis, Paris IX Dauphine, France, 1996.

[8] D. Colton, A. Kirsch, and L. Päivärinta. Far-field patterns for acoustic waves in an inhomogeneous medium. *SIAM J. Math. Anal.*, 20(6):1472–1483, 1989.

[9] D. Colton and R. Kress. *Inverse acoustic and electromagnetic scattering theory.* Springer, 3rd edition, 2013.

[10] D. Colton and P. Monk. The inverse scattering problem for time-harmonic acoustic waves in an inhomogeneous medium. *Quart. J. Mech. Appl. Math.*, 41:97–125, 1988.

[11] D. Colton, L. Päivärinta, and J. Sylvester. The interior transmission problem. *Inverse Problems and Imaging*, 1:13–28, 2007.

[12] A. Cossonnière. *Valeurs propres de transmission et leur utilisation dans l'identification d'inclusions à partir de mesures électromagnétiques.* PhD thesis, Université de Toulouse, 2011.

[13] A. Cossonnière and H. Haddar. Surface integral formulation of the interior transmission problem. *J. Integral Equations Applications*, 25(3):341–376, 09 2013.

[14] J.-P. Eckmann and C.-A. Pillet. Spectral duality for planar billiards. *Commun. Math. Phys.*, pages 283–313, 1995.

[15] K. Hickmann. Interior transmission eigenvalue problem with refractive index having C^2-transition to the background medium. *Appl. Anal.*, 91(9):1675–1690, 2012.

[16] X. Ji and J. Sun. A multilevel finite element method for transmission eigenvalues of anisotropic media. *J. Comput. Phys.*, 255:422–435, 2013.

[17] X. Ji, J. Sun, and H. Xie. A multigrid method for Helmholtz transmission eigenvalue problems. *J. Sci. Comput.*, 60(2):276–294, 2014.

[18] Z. Jiang and A. Lechleiter. Computing interior eigenvalues of domains from far fields. *IMA Journal of Numerical Analysis*, 2015.

[19] A. Kirsch. The denseness of the far field patterns for the transmission problem. *IMA Journal of Applied Mathematics*, 37:213–225, 1986.

[20] A. Kirsch and N. I. Grinberg. *The Factorization Method for Inverse Problems.* Oxford Lecture Series in Mathematics and its Applications 36. Oxford University Press, 2008.

[21] A. Kirsch and A. Kleefeld. The factorization method for a conductive boundary condition. *J. Integral Equations Appl.*, 24(4):575–601, 2012.

[22] A. Kirsch and A. Lechleiter. The inside-outside duality for scattering problems by inhomogeneous media. *Inverse Problems*, 29(10):104011, 2013.

[23] A. Kleefeld. *Direct and inverse acoustic scattering for three-dimensional surfaces.* PhD thesis, University of Wisconsin – Milwaukee, USA, 2009.

[24] A. Kleefeld. The exterior problem for the Helmholtz equation with mixed boundary conditions in three dimensions. *Int. J. Comput. Math.*, 89(17):2392–2409, 2012.

[25] A. Kleefeld. A modified boundary integral equation for solving the exterior Robin problem for the Helmholtz equation in three dimensions. *Appl. Math. Comput.*, 219(4):2114–2123, 2012.

[26] A. Kleefeld. The transmission problem for the Helmholtz equation in $\mathbb{R}^3$. *Comput. Methods Appl. Math.*, 12(3):330–350, 2012.

[27] A. Kleefeld. A numerical method to compute interior transmission eigenvalues. *Inverse Problems*, 29(10):104012, 2013.

[28] A. Kleefeld. Numerical methods for acoustic and electromagnetic scattering: Transmission boundary-value problems, interior transmission eigenvalues, and the factorization method. Habilitation thesis, Brandenburg University of Technology Cottbus - Senftenberg, Cottbus, 2015.

[29] A. Kleefeld and T.-C. Lin. The nonlinear Landweber method applied to an inverse scattering problem for sound-soft obstacles in 3D. *Comput. Phys. Comm.*, 182(12):2550–2560, 2011.

[30] A. Kleefeld and T.-C. Lin. Boundary element collocation method for solving the exterior Neumann problem for Helmholtz's equation in three dimensions. *Electron. Trans. Numer. Anal.*, 39:113–143, 2012.

[31] A. Lechleiter and S. Peters. Analytical characterization and numerical approximation of interior eigenvalues for impenetrable scatterers from far fields. *Inverse Problems*, 30(4):045006, 2014.

[32] A. Lechleiter and S. Peters. Determining transmission eigenvalues of anisotropic inhomogeneous media from far field data. *Commun. Math. Sci.*, 13(7):1803–1827, 2015.

[33] A. Lechleiter and M. Rennoch. Inside-outside duality and the determination of electromagnetic interior transmission eigenvalues. *SIAM J. Math. Anal.*, 47(1):684–705, 2015.

[34] W. McLean. *Strongly Elliptic Systems and Boundary Integral Operators*. Cambridge University Press, Cambridge, UK, 2000.

[35] P. Monk and J. Sun. Finite element methods for Maxwell's transmission eigenvalues. *SIAM J. Sci. Comput.*, 34(3):B247–B264, 2012.

[36] L. Päivärinta and J. Sylvester. Transmission eigenvalues. *SIAM Journal on Mathematical Analysis*, 40(2):738–753, 2008.

[37] B. P. Rynne and B. D. Sleeman. The interior transmission problem and inverse scattering from inhomogeneous media. *SIAM J. Math. Anal.*, 22(6):1755–1762, 1991.

[38] J. Sun and L. Xu. Computation of Maxwell's transmission eigenvalues and its applications in inverse medium problems. *Inverse Problems*, 29(10):104013, 18, 2013.

[39] A. Tamburrino, S. Ventre, and G. Rubinacci. Recent developments of a monotonicity imaging method for magnetic induction tomography in the small skin-depth regime. *Inverse Problems*, 26:074016 (21pp), 2010.